



From mountain summits to roots: Crustal structure of the Eastern Alps and Bohemian Massif along longitude 13.3°E

György Hetényi^{a,b,c,d,*}, Jaroslava Plomerová^e, Irene Bianchi^f, Hana Kampfová Exnerová^e, Götz Bokelmann^f, Mark R. Handy^g, Vladislav Babuška^e, AlpArray-EASI Working Group

^a Institute of Earth Sciences, University of Lausanne, Lausanne, Switzerland

^b Institute of Geophysics, Department of Earth Sciences, ETH Zürich, Zürich, Switzerland

^c Swiss Seismological Service, ETH Zürich, Zürich, Switzerland

^d Geodetic and Geophysical Institute, Research Centre for Astronomy and Earth Sciences, Hungarian Academy of Sciences, Sopron, Hungary

^e Geophysical Institute, Czech Academy of Sciences, Prague, Czech Republic

^f Department of Meteorology and Geophysics, University of Vienna, Vienna, Austria

^g Freie Universität Berlin, Berlin, Germany

ARTICLE INFO

Keywords:

Seismology
Crust
Receiver functions
Eastern Alps
Bohemian Massif
Tauern Window

ABSTRACT

The crustal structure of the Eastern Alps and adjacent tectonic units investigated in this work sheds new light on the relationship of surface geology to geodynamic processes operating at depth. Of particular interest are the nature of a previously proposed Moho gap south and east of the Tauern Window, the plate tectonic affinity of the steeply dipping Eastern Alpine slab, and the relationship of the Alps to the Neogene sedimentary basins and the Bohemian Massif. To address these questions, we use various seismological approaches based on converted waves from the temporary passive experiment EASI (Eastern Alpine Seismic Investigation), a complementary experiment of the AlpArray project. The EASI is a densely spaced, 540 km long seismic network along 13.3°E we operated for more than a year. The uppermost-crustal structures in and near the Alps exhibit dipping layers and/or tilted anisotropy that correlate well with surface geology observations. The Moho, despite its variable appearance, is clearly identified along most of the swath. The Variscan lithospheric blocks beneath the Bohemian Massif are imaged with sub-vertical boundaries. Beneath the Eastern Alps, the shape of the Moho is consistent with bi-vergent orogenic thickening, with a steeper and deeper-reaching Adriatic plate plunging northwards beneath the European plate in the north. At the junction of these plates at depth, around the previously proposed Moho gap, the root of the Eastern Alps is a broad trough characterized by a zone of low velocity-gradient that is up to 20 km thick, transitioning between crust and mantle. Our receiver-function results corroborate earlier lithosphere-upper mantle seismic tomography images, and highlight the Adriatic affinity of the Eastern Alpine slab. The zigzag deployment pattern of stations in the EASI experiment also allows distinction of short-wavelength variations perpendicular to the profile, both within the shallow and the deep crust. This underlines the importance of applying 3D imaging in complex geodynamic systems.

1. Introduction

The Alps are relatively short in comparison with other mountain ranges such as the Himalayas or the Andes, but they are extremely complex with pronounced along-strike changes in structure. The topography in their western, arcuate part developed above the downgoing Eurasia plate. Present seismicity and deformation rate are relatively low, reflecting the location of the current rotation pole of Adria with respect to Europe in the north-western Alps (e.g., Weber et al., 2010). The eastern, straight part of the Alps has lower relief than the Western

Alps. The origin of the downgoing slab(s) beneath the Eastern Alps is controversial, with most major historical earthquakes of the last millennium concentrated on its southern edge (see below and Fig. 1). The collisional evolution of the Alps between Europe and Africa involved several microplates that are partly responsible for the structural complexity (e.g., Handy et al., 2015 and references therein). Another aspect of the Alps is the along-strike variability of the adjacent European plate: from the Massif Central to the Jura Mountains in the west, over the Molasse Basin in the centre, to the lithospheric blocks of the Bohemian Massif, the collision encountered various boundary conditions.

* Corresponding author.

E-mail address: gyorgy.hetenyi@unil.ch (G. Hetényi).

<https://doi.org/10.1016/j.tecto.2018.07.001>

Received 17 March 2018; Received in revised form 31 May 2018; Accepted 3 July 2018

Available online 05 July 2018

0040-1951/ © 2018 The Author(s). Published by Elsevier B.V. This is an open access article under the CC BY-NC-ND license

(<http://creativecommons.org/licenses/by-nc-nd/4.0/>).

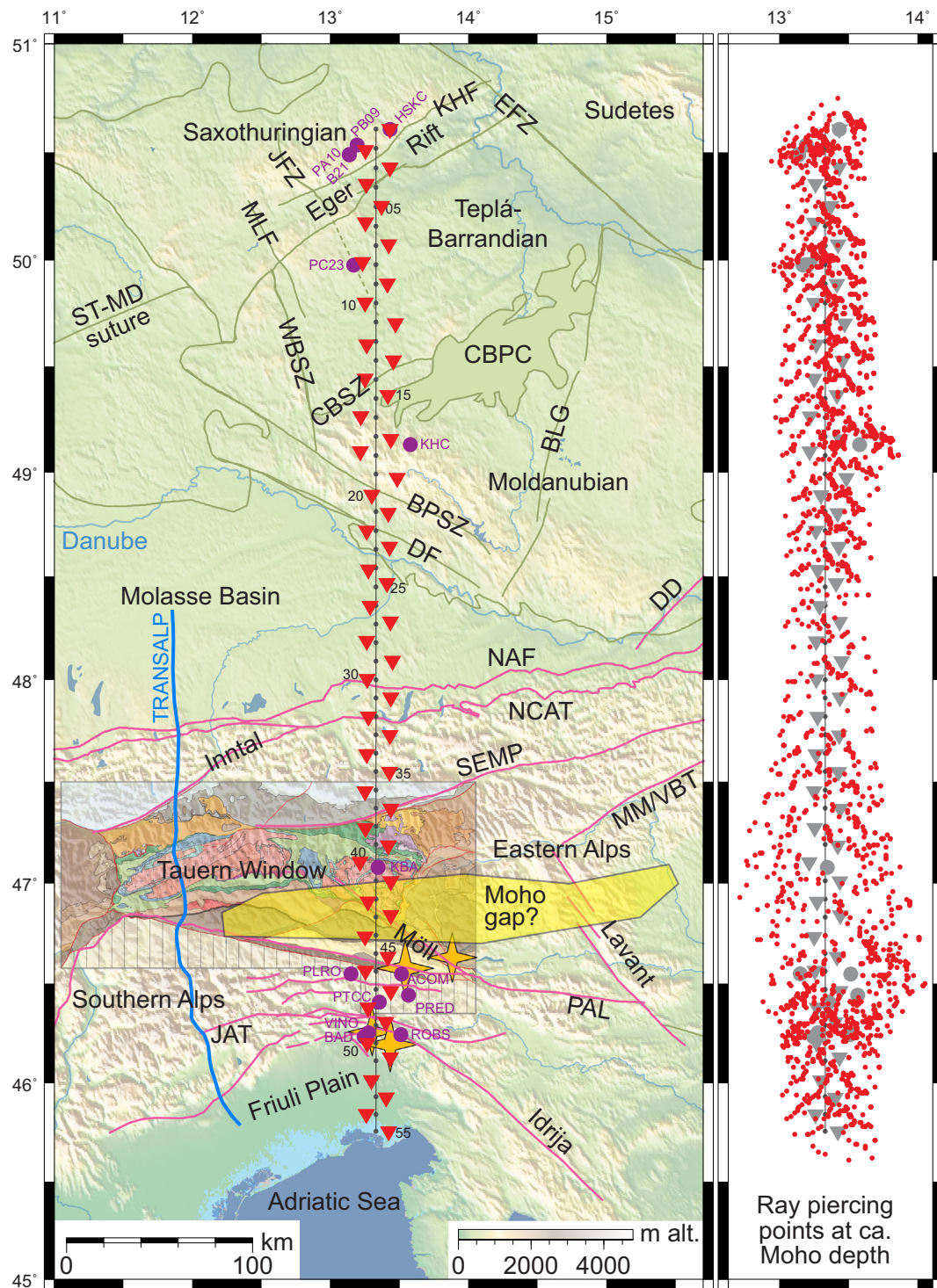


Fig. 1. Left: Geographical, geological and geophysical setting. Seismological stations used in this study are shown as red triangles (55 EASI temporary stations) and purple circles (14 permanent or past temporary stations near the profile, with names). Central black line with dots every 10 km is for reference, starting at longitude 50.60745°N (northernmost station). The TRANSALP experiment location is outlined in blue. Main blocks of the Bohemian Massif are shown with green contours and shading. The Tauern Window geological map is from Schmid et al. (2013). Main faults are shown in pink. Yellow stars show the location of major earthquakes mentioned in the text. The yellow zone locates the “Moho gap” (according to Spada et al., 2013), one of the main targets for imaging as described in the main text. Abbreviations: BLG – Blanice Graben, BPSZ – Bavarian Pfahl Shear zone, CBPC – Central Bohemian Pluton Complex, CBSZ – Central Bohemian Shear Zone, DD – Dindorf Fault, DF – Danube Fault, EFZ – Elbe Fault Zone, JAT – Julian Alps Thrust, JFZ – Jáchymov Fault Zone, KHF – Krušné Hory Fault, Möll – Mölltal Fault, NAF – Northern Alpine Fault, NCAT – Northern Calcareous Alps Thrust, MLF – Mariánské Lázně Fault, MM/VBT – Mur-Mürz/Vienna Basin Transfer fault, PAL – Periadriatic Line, SEMP – Salzach–Ennstal–Mariazell–Puchberg fault, ST-MD – Saxothuringian–Moldanubian, WBSZ – West Bohemian Shear Zone. (For interpretation of the references to colour in this figure legend, the reader is referred to the web version of this article.)

Much of our knowledge of the deep structure of the Eastern Alps comes from seismological experiments such as TRANSALP (e.g., TRANSALP Working Group, 2002), ALPASS (Mitterbauer et al., 2011), BOHEMA III (Karousová et al., 2013) and ALP (Brückl et al., 2007). The TRANSALP experiment involved both active and passive seismic methods (TRANSALP Working Group, 2002). Whereas the active seismics imaged a major south-dipping ramp starting from the surface and reaching the centre of the orogen, as well as bi-vergent crustal thickening, TRANSALP provided no conclusive constraints on the geometry of the deep contact of the European and Adriatic plates. Two models were proposed: (1) the “Crocodile model” in which European crust wedges deeply to the south into the Adriatic plate; and (2) the “Lateral extrusion model” in which the plate was interpreted to extend steeply downwards from the Periadriatic Lineament to the base of the crust (for details, see TRANSALP Working Group, 2002; Castellarin et al., 2003; Kummerow et al., 2004; Lüschen et al., 2004; Bleibinhaus and Gebrande, 2006; Ortner et al., 2006; Lammerer et al., 2008). Further east of the TRANSALP section, the longer Alp01 active seismic line (e.g., Brückl et al., 2007) had limited depth penetration beneath the Moho, and although it resolved crustal velocities, it did not shed light on the relationship between the two plates at depth. Passive seismic methods based on receiver functions provide an adequate tool to fill the image gap, but past attempts were hampered by sparse station coverage and to single-station methodologies or imaged the Moho, crustal anisotropy, and the lithosphere-asthenosphere boundary (LAB) in a pointwise manner (Babuška and Plomerová, 1992; Bianchi et al., 2015; Bianchi and Bokelmann, 2014; Bianchi et al., 2014). Therefore, knowledge about the connection of the crustal structure with the subducting slabs as imaged by P-wave tomography (e.g., Babuška et al., 1990; Lippitsch et al., 2003; Mitterbauer et al., 2011; Dando et al., 2011) and their accumulation in the mantle-transition zone beneath the broader Alpine region (e.g., Lombardi et al., 2009; Hetényi et al., 2009; Dando et al., 2011) remains poor. This calls for imaging with denser seismological networks and with methods that take advantage of ray crossing beneath the network.

While the Alps are now being scrutinized by the dense seismological network of the AlpArray project (Hetényi et al., 2018), several complementary experiments within the AlpArray project target more specific regions at higher resolution. The Eastern Alpine Seismic Investigation (EASI) experiment, presented here, focuses on the structure of the Alps and adjacent areas along a north-south transect at ca. 13–13.5°E, i.e., between the former TRANSALP and ALPASS (e.g., Mitterbauer et al., 2011) experiments. The swath of stations in EASI extends from the Czech-German border, north of the Eger Rift, to the coast of the Adriatic Sea, in the Friuli Plain, with an average station spacing of 10 km (Fig. 1). Beyond shedding light on the origin of the downgoing slab beneath the Eastern Alps, project EASI also aims at imaging the structural connection between the Alps, both foreland basins, and the lithospheric blocks of the Bohemian Massif. Within the crust, we search for signs of anisotropy and lateral variability of structures, and focus also on shallow targets such as the sedimentary infill. Of particular interest is the Tauern Window (Fig. 1), one of the most emblematic tectonic structures, providing an particular opening to expose middle-grade metamorphic rocks of the middle crust of European affinity and Cenozoic age, in the midst of Cretaceous and Adriatic rocks of similar metamorphic signature (e.g., Schuster et al., 2004). The roots of this region and of the associated relief are still not well-understood and have been suggested to be devoid of a clear Moho signal (see Section 2.3). Our new receiver-function images, complemented with other seismological data and geological information, provide a refined and improved image of the crust along 13.3°E between ca. 45.5 and 50.5°N, and may also help explain why the southern part of this area has hosted the largest Alpine earthquakes in human history.

2. Geodynamic setting

The EASI experiment's stations are deployed in a double-line geometry along longitude 13.33°E that crosses several well-known and -described geological units (Fig. 1).

2.1. The Bohemian Massif

The northern half of the station network crosses the SW-NE oriented structures of the Bohemian Massif, a mosaic of several microplates (Plomerová et al., 2007) amalgamated during the Variscan orogeny (Matte et al., 1990). From north to south, the profile cuts three main tectonic units of the massif: the Saxothuringian (ST), Teplá-Barrandian (TB) and the Moldanubian (MD). The original microplates were accreted in a broad collisional zone between the major plates, Gondwana and Laurussia. Convergence of these two supercontinental plates resulted in closure of small oceanic basins and in multiple accretion, subduction and collisional events along the margins of the neighbouring microplates. For review of a plate-kinematic model of the assembly of the Bohemian Massif, we refer to Žák et al. (2014).

The linear EASI profile cuts sutures between the lithospheric blocks as well as several distinct faults. The suture between the Saxothuringian (ST) and the Teplá-Barrandian (TB) units was the locus of both oceanic and continental subductions, expressed by the Krušné Hory Fault (KHF) at the surface (Fig. 1). The suture is steep both in the crust (Mlčoch and Konopásek, 2010) and in the mantle lithosphere (Babuška et al., 2010). The geodynamically active Eger (Ohře) Rift, accompanied by a substantial Cenozoic volcanism, developed along this suture. Unlike the ST/TB suture, the boundary between the Teplá-Barrandian and the Moldanubian units (Central Bohemian Shear Zone, CBSZ) is modelled as an inclined suture (Babuška and Plomerová, 2013) that probably provided a weakened path for multiple intrusions of the Central Bohemian Plutonic Complex (CBPC) (Fig. 1). In contrast to the orogen-parallel boundaries mentioned above (KHF, CBSZ), the Jáchymov Fault Zone (JFZ) is the broad, NW-SE trending orogen-perpendicular system of faults running from the Saxothuringian towards the Moldanubian unit. Its south-eastward continuation, though not generally accepted, is supported by weak seismic activity in the South-Bohemian Cenozoic basins (Lenhardt et al., 2007). Some authors assume that the Moldanubian unit also forms the southernmost part of the present European plate beneath the Molasse Basin and the northern rim of the Alps.

To the southwest, the crust of the Bohemian Massif is rimmed by a NW-SE trending fault system comprising the Bavarian Pfahl Shear Zone (BPSZ) and by the Danube Fault (DF). Both fault systems, characterized by a dextral sense of displacement, represent sediment-filled strike-slip zones initiated during the late Paleozoic (Mattern, 2001; Siebel et al., 2005). Mineralization of both fault zones indicates that the system was also active after the Permian stabilization of the Bohemian Massif. Apatite fission-track data indicate Triassic tectonic activity, though the vertical offset of Mesozoic strata on the Danube Fault further proves its post-Permian reactivation (Siebel et al., 2010).

2.2. The Alps

The Eastern Alps follow the strike of the collision between the European and Adriatic plates. Nappe stacking and crustal thickening in the Eastern Alps began in late Cretaceous time (also known as the Eo-Alpine phase), and was followed by a second, Tertiary phase (Schmid et al., 1996). The orogenic structure of the Eastern Alps was modified in Neogene time by northward indentation of the Adriatic plate and eastward retreat of the European slab beneath the Carpathians (Royden et al., 1982; Royden and Burchfiel, 1989), which effected E-W directed thinning and lateral eastward extrusion of the Alpine orogenic edifice

towards the Pannonian Basin (Ratschbacher et al., 1991; Fügenschuh et al., 1997; Rosenberg et al., 2007; Scharf et al., 2013; Schmid et al., 2013). This process exhumed Penninic units in the Tauern Window, considered to be the most striking tectonic feature of the Eastern Alps (Frisch et al., 2000; Bertrand et al., 2017; Favaro et al., 2017).

Faults and tectonic units relevant for this study are shown in Fig. 1 and described below from north to south:

- The foreland Molasse Basin on top of the crystalline basement forming the southern continuation of the Bohemian Massif.
- Sediments of the Subalpine Molasse are folded and imbricated the Northern Calcareous Alps (NCA) and define the Northern Alps Front (NAF).
- The NCA are far-travelled nappes derived from Austroalpine basement south of the Tauern Window (Schuster et al., 2004; Schmid et al., 2004; Handy et al., 2010) and emplaced along their basal thrust onto European-derived units along the Northern Calcareous Alps Thrust (NCAT). The NCA experienced Neogene E-W extension along mostly dextral strike-slip faults, including the Inntal fault, that separates the western and central part of the NCA.
- The Salzachtal-Ennstal-Mariazell-Puchberg fault (SEMP) bounds the Tauern Window (TW) to the north.
- The dextral Mölltal fault zone is a shear zone bounding the south-eastern part of the TW from the Austroalpine basement.
- The Periadriatic Lineament (PAL), a 700 km long fault system that separates the Southern Alps from the main body of the Alps (Schmid et al., 1989); it comprises two segments: West of the sinistral Giudicarie Line (GL), the PAL is an Oligo-Miocene transpressive fault that accommodated ca. 150 km dextral strike-slip and backthrusting of the Alpine metamorphic edifice onto the unmetamorphic Southern Alpine units (Schmid et al., 1989); East of the GL, it is a Neogene dextral strike-slip fault that overprints the older Oligocene fault mentioned above. Neogene displacement on this eastern segment increases eastward from zero at its junction with the GL to several tens of kilometres (Handy et al., 2005; Scharf et al., 2013).
- The Southern Alps are located south of the PAL (e.g., Castellarin and Cantelli, 2000).

The EASI profile terminates in the Friuli Plain, the southern Mio- to Pleistocene foreland of the Southern Alps bordering the Adriatic Sea.

2.3. Seismological context

The entire study region has been the topic of numerous, albeit incomplete seismological investigations. Here we highlight the most important ones related to the EASI project.

The outlines and origin of a slab anomaly beneath the Eastern Alps are the subject of ongoing controversy. Proponents of a N-dipping Adriatic subduction (Lippitsch et al., 2003; Schmid et al., 2004; Kissling et al., 2006) argue that this configuration started forming at ca. 21 Ma with a subduction polarity reversal, following breakoff of the south-dipping, late Cretaceous-late Eocene European slab. On the other hand, advocates of a European origin of this slab anomaly (Mitterbauer et al., 2011) argue that this polarity reversal has never happened; instead they attribute the steep, N-ward dip of the slab anomaly to bending and roll-over of the European slab. The debate is complemented with suggestions on a dual origin of the steep north-dipping slab (Babuška et al., 1990), also further east (Handy et al., 2015). Solving the controversial origin of the slab beneath the Eastern Alps is relevant for the Friuli seismic hazard area, which, depending on the subduction polarity, is located in the foreland (if the Eastern Alps slab is Adriatic) or in the hinterland of the Alps (if the slab is European).

South and east of the Tauern Window is a peculiar feature known as the “Moho gap” (Fig. 1). While the Moho is clearly documented beneath most of the Tauern Window (e.g., Lüschen et al., 2006), Bleibinhaus and Gebrande (2006) first noted a possible gap between the European

and the Adriatic Mohos based on wide-angle reflections along fan profiles. This gap is ca. 250 km long by ca. 30 km wide and is elongated in an E-W direction. Behm et al. (2007) described this zone as a region with no or very weak refracted *Pn* phases, due to “fragmentation of the Moho or lack of data”, as observed in active seismic experiments. The same region was later probed with reflected *PmP* phases by Spada et al. (2013), who further outlined the Moho gap. In the lack of strong constraints, the Moho gap is also reported in the large, regional Moho depth compilation of Spada et al. (2013). Sampling this “Moho gap” zone with receiver functions was one of the main motivations of the EASI experiment. The RFs, analogous to *PmP* wide-angle complete reflections, are sensitive to the strength of the first-order velocity discontinuity of the interface and also to velocity gradients.

Another key structure interpreted from observations in the TRANSALP experiment (TRANSALP Working Group, 2002), ca. 100 km to the west of the EASI profile, is the moderately southward-dipping thrust beneath the Tauern Window, the so-called Sub-Tauern Ramp (STR). This feature was better imaged by reflection seismics than by receiver functions (Kummerow et al., 2004). The STR is proposed to connect with the Inntal fault system at surface at that longitude (Ortner et al., 2006). Nearly symmetrically, another thrust fault dipping to the N as imaged by both seismic methods, the Sub-Dolomites Ramp beneath the Southern Alps is underlain by an intracrustal interface, named the Adriatic Crustal Interface (ACI) (Kummerow et al., 2004).

The Southern Alps at the longitude of the EASI profile have hosted 4 of the 7 largest earthquakes of the Alpine region in the last millennium (Fig. 1 yellow stars): the 1348 M7.0 Villach, the 1511 M6.9 Idrija, the 1690 M6.6 Carinthia earthquakes (details in Stucchi et al., 2012) and the 1976 M6.5 Friuli mainshock (ISC, 2015). The structures imaged in the Alpine part of our profile are of special importance in defining and controlling the geometries of faults hosting major seismic events.

3. Data and methods

3.1. The EASI network

The Eastern Alpine Seismic Investigation project is a Complementary Experiment of the AlpArray project. Staggered funding of national AlpArray projects made possible the deployment of 55 broadband seismometers between the summers of 2014 and 2015 to carry out the EASI. The stations are deployed at a uniform, 10 km spacing along a N-S transect, with alternating deployments 6 km to the west and east of the central line. This resulted in a zigzag pattern along the swath. We aimed to keep sites within 1.5 km of planned locations. This value ended up as the average shift between planned and actual sites, with distances ranging from 0.16 to 4.4 km. The stations were installed at elevations between 1 and 1909 m above sea-level (average: 666 m). The EASI swath traversed the Eger Rift, then near Plzeň, Passau, Salzburg, through the eastern part of the Tauern Window, through Gmünd in Kärnten, near Udine, reaching the Adriatic Sea (Fig. 1). Station coordinates and information are provided under the Digital Object Identifier 10.12686/alparray/xt_2014.

All sites were equipped with broadband seismometers: twenty-eight STS-2 (120 s corner period), fifteen Trillium Compact (120 s), eight Reftek151 (60 s), two CMG-3ESP (30 s), one CMG-3T (120 s) and one CMG-40T (120 s). The stations recorded in continuous mode collecting 100 samples per second. The station names started with “AAE”, completed by “01” to “55” between the northernmost and southernmost site. The EASI experiment’s network code is XT, and data will be available to the public in autumn 2018 through the Swiss Seismological Service’s archive.

For the part of our analysis focusing on crustal structure with receiver-function migration, we also included data from permanent and past temporary stations in the immediate vicinity of the EASI swath. These additional 14 stations are labelled in Fig. 1 and helped to clearly identify some of the complex structures imaged beneath the Alps. This is well-represented by the piercing point coverage (Fig. 1) at the final deduced Moho depth.

3.2. Data selection

Teleseismic data from earthquakes at 30–90° epicentral distance and magnitude 5.5 and above were selected from the USGS catalogue for receiver-function analysis, resulting in 199 events and 8254 traces for the EASI stations. For the additional stations used for migration, data was downloaded between August 2002 and March 2017, resulting in 2029 events and 7385 traces. The overall distribution of teleseismic event magnitudes, epicentral distance and back-azimuths is shown in Fig. S1.

The selection of seismological data was slightly different for the various analyses, as described below, and in general included quality control using several steps. The details are provided in the next sections. In general, we used the Z-R-T coordinate system, unless otherwise noted.

3.3. Receiver-function analyses

Receiver functions (RF) exploit mode-converted waves to unravel discontinuities at depth, and to infer the v_S and v_P/v_S of the layers above them. The technique has become a standard tool for the analysis and interpretation of seismological data (for an overview, see e.g. Kind and Yuan, 2011). Here, we briefly describe the multi-method approaches to analyse EASI data for imaging shallow structure of the crust down to the Moho beneath different tectonic units represented by the Variscan Bohemian massif, Alpine foreland basins and the Alpine collisional zone itself.

3.3.1. Harmonic analysis

In complex tectonic environments such as orogens, the signal detected on both the radial (R) and transverse (T) components of the RF is strong; here we analyse both components simultaneously by the application of the harmonic expansion, with the aim of providing details on the shallowest part of the crust.

First, teleseismic traces with impulsive and visible direct P-wave arrival, incoming on the 30–90° epicentral distance range, have been visually selected. After rotation into the Z-R-T coordinate system we follow the approach developed by Park and Levin (2000) for the computation of the RF, which makes use of a frequency domain algorithm using multi-taper correlation estimates to minimize spectral leakage and its frequency dependent down-weighting.

Details on the back-azimuthal harmonic decomposition analysis can be found in Bianchi et al. (2010). This technique lets the RF be decomposed into a sum of $\cos(k\phi)$ and $\sin(k\phi)$ functions, where k is the harmonics degree and order, and ϕ is the back-azimuth. The analysis is here limited to the first two harmonic orders ($k = 0$, and $k = 1$). The $k = 0$ component is also called the “constant component”: it retains isotropic variations of seismic velocities at depth due to the null contribution of the transverse RF. On the other hand, the $k = 1$ components isolate the energy appearing with 2π periodicity within back-azimuthal sweeps. The 2π periodicity is generated by dipping interfaces or anisotropy with tilted symmetry axis (see also Maupin and Park, 2007). The $k = 1$ components are the weighted sums of the R- and T- components of the RF according to the back-azimuth considering the $\pi/2$ shift of the energy on the transverse RF with respect to the radial RF (Shiomi and Park, 2008).

For the EASI dataset, single RFs are migrated to 10 km depth using PREM velocities (Dziewonski and Anderson, 1981), and then stacked for station gathers; a frequency filter of 2 Hz is applied to help recognizing fine shallow structures (Fig. 2a). The amplitude, defined as the sum of the squared values of the two $k = 1$ components (cosine and sine) (Fig. 2b), shows the depth and location of non-horizontal structures, highlighting the presence of dipping interfaces or anisotropy with tilted axis. The results of this approach are described in Section 4.1. Further information on the whole crustal structure beneath EASI transect, from harmonics analysis and focusing at larger depths, is shown in Fig. S2 of the supplementary material.

3.3.2. Single-station approaches

P-to-S converted RF stations stacks represent the simplest method of Moho depth and average crustal v_P/v_S estimates. Teleseismic events with a lower cut-off magnitude of

$$M_c = 5.2 + (\Delta - 30)/(180 - 30) - D/700$$

were selected, where Δ is epicentral distance and D is focal depth in km (Liu and Gao, 2010). Then the signal-to-noise ratio (SNR) was tested on all Z-components band-pass filtered at 1–8 s and only signals with

$$\text{SNR} = (A_{2\text{max}} - A_{2\text{min}})/(A_{1\text{max}} - A_{1\text{min}}) > 2.5$$

were further analysed. Amplitudes A_1 and A_2 were measured in the 30 s time interval before and 30 s window after the direct P-wave arrival (calculated according to *iasp91*, Kennett et al., 1995). To rotate the selected raw signals into the ray-oriented L-Q-T coordinate system, we use the TauP Toolkit (Crotwell et al., 1999) for determining theoretical back-azimuths and incidences assuming the *iasp91* Earth reference velocity model. Then, the P-to-S receiver functions were calculated using the PRF-LQT-N.SHC script (Kind et al., 1995; Kind and Yuan, 2011) based on deconvolution method by Berkhout (1977). The inverse filter is generated in the time domain from the P waveform on the L component, containing mainly the SV energy of converted waves, by minimizing the least-square difference between the actual output and the desired delta-like spike function of normalized amplitude. All components are normalized to the maximum of the L component. To improve the signal-to-noise ratio we sum the RF traces from a broad range of epicentral distances and back-azimuths, after moving-out individual receiver functions into reference distance of 66° (slowness 6.4 s/°). An advantage of receiver functions calculated in the L-Q-T system comes from the zero amplitude in the P-wave arrival time. Non-zero amplitudes of receiver functions calculated in the Z-R-T coordinate system tend to mask conversions from shallow sedimentary layers (e.g., in the Molasse Basin, in our case). Moreover, non-zero amplitude on the receiver functions at zero time is in sign of a technical problem, e.g., an incorrect orientation of seismometer or gains of individual components of the station (Vecsey et al., 2017). One also has to consider potential effects from differences between the theoretical and dynamic back-azimuth-incidences pairs for signal rotation due to local near-surface structures. Several filters were applied on the evaluated receiver functions in our search of the respective converters. The forward-and-reverse 4th order Butterworth filter in the 1–8 s period range provided the RF with the most distinct converted phases up to ~20 s after the direct P arrival. The results of this approach are shown in Fig. 3.

The frequently used Zhu and Kanamori (2000) h_M - v_P/v_S (also known as H- κ) method searches for optimal pairs of h_M and average crustal v_P/v_S ratio to produce synthetics that fit the observed RF waveforms. The method yields a powerful first estimate of both values provided the sensitive assumptions are close to reality: flat discontinuities with a sharp velocity contrast and realistic assumed crustal v_P . If these are not fulfilled, several local maxima occur in the h_M - v_P/v_S space and the ad hoc selected weights of the Ps, PpPs and PpSs + PsPs (from now on: PpSs) phases determine the result. We have applied this method on observed RF calculated using the code of Helffrich et al. (2013) with the parameters as follows: average crustal $v_P = 6.1$ km/s (as in *iasp91*), slowness of 6.4 s/°, equal weights of the converted phases (1:1:1).

A similar, even simpler approach is to estimate the Moho depth using differential travel times. The most straightforward is to pick Ps–P travel time Δt_1 and to convert it into a depth using a velocity model. We picked the Δt_1 times from stacks of individual RF traces filtered at 0.125–1 Hz and used the *iasp91* velocity model for the time-to-depth conversion. Considering a standard ray parameter of 6.4 s/°, this results in a time-to-depth conversion of

$$h_M = 8.36 \cdot \Delta t_1 \cdot 0.94,$$

where the 8.36 and 0.94 multipliers account for the difference between

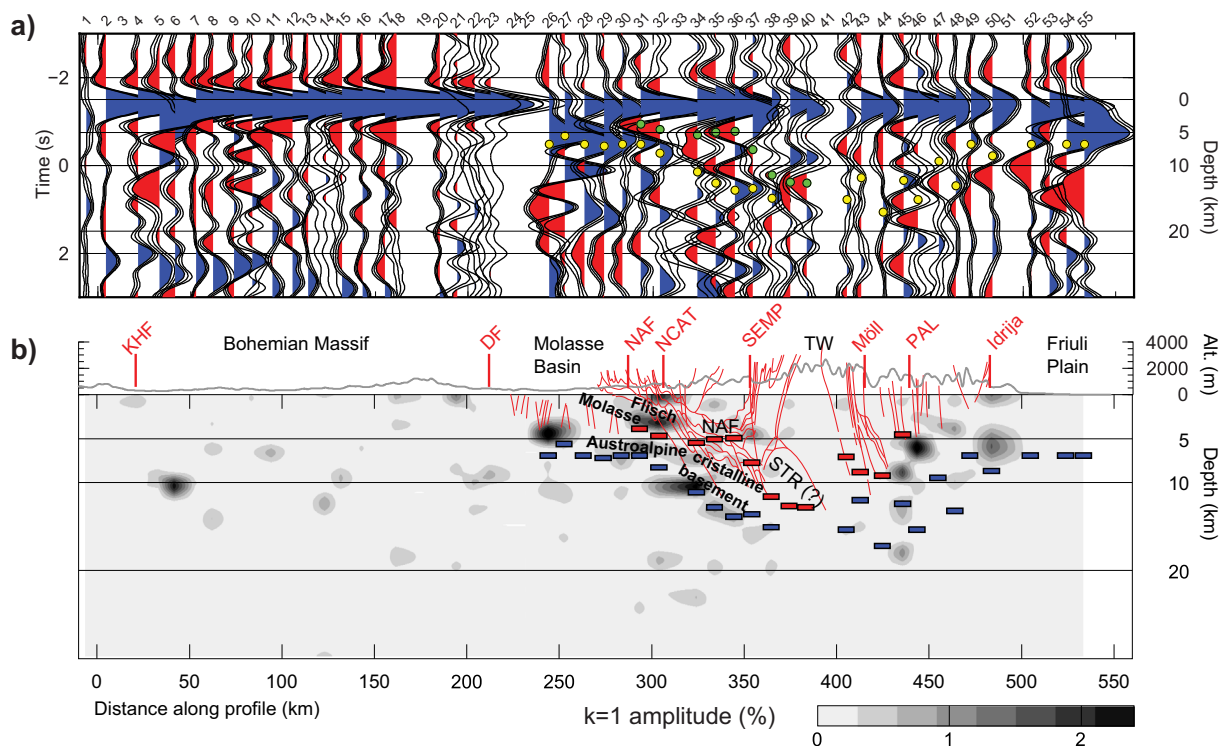


Fig. 2. Shallow structure from the harmonics analysis of single station receiver functions. (a) The constant ($k = 0$) component of the harmonic expansion of RFs. Blue and red pulses indicate positive and negative amplitudes, respectively. Green (resp. yellow) dots highlight the picked extreme amplitudes of the negative (resp. positive) pulses beneath the corresponding stations. Due to the depth migration, zero time here corresponds to 10 km depth, which allows to highlight the features at ± 10 km around the focus depth. (b) Topographic profile and major faults of the area, with abbreviations as on Fig. 1. Background grayscale image corresponds to the sum of the energy on the two $k = 1$ terms from harmonic analysis at each station, displayed along the profile. Red resp. blue rectangles refer to the picked negative resp. positive amplitudes from the constant component shown in (a). The fault overlay is from the geological profile at the corresponding longitude (Egger et al., 1999). STR – Sub-Tauern-Ramp, TW – Tauern Window. (For interpretation of the references to colour in this figure legend, the reader is referred to the web version of this article.)

average v_p and v_s in the crust and for slowness given the upper crustal velocity model. Likewise, clear multiples on the RF traces can be exploited for an independent estimate of Moho depth, although they average the structure over a larger volume beneath a station compared to the previous one:

$$h_M = 8.36 \cdot \Delta t_3 \cdot 0.94,$$

where Δt_3 is the PpSs–PpPs differential time. Assuming that the ray parameter $p^2 < 1/v$ (Chevrot and Girardin, 2000), we can estimate the average crustal v_p/v_s as

$$v_p/v_s \sim (\Delta t_2/\Delta t_1 + 1)/(\Delta t_2/\Delta t_1 - 1),$$

where Δt_2 is the PpPs–P differential time, and, analogously to depth estimates, also

$$v_p/v_s \sim (\Delta t_2/\Delta t_3 + 1)/(\Delta t_2/\Delta t_3 - 1)$$

(Zandt et al., 1995; Zandt and Ammon, 1995).

Moreover, in case of picking the Ps as well as the multiple phases we can use the above equations and verify whether the times of interpreted phases correspond to conversions on the same discontinuity, in our case to the Moho. The h_M depths for measured differential times, Δt_1 , Δt_2 , Δt_4 (the last one stems from differential time of PpSs–P) were calculated for v_p/v_s in the 1.5–2.0 interval, with $v_p = 6.1$ km/s and slowness 6.4 s°. The intersection point of the three curves, or, barycentre of the three very close intersections are considered as the best-fitting h_{M-v_p/v_s} pair beneath the station. Results of this approach and comparison with other techniques are described in Section 4.2 and shown in Fig. 4.

3.3.3. Migration

We employ pre-stack RF migration for true reconstruction of

converter geometries at depth. The RFs for this purpose were calculated in the Z-R-T coordinate system filtered in the 0.125–1 Hz frequency band, using the time-domain iterative deconvolution of Ligorria and Ammon (1999) with 150 iterations, and then convolved with a Gaussian of width corresponding to the higher corner frequency of the previous filter (1 Hz). The resulting radial and transverse RFs sorted by ranges of back-azimuth are shown for all stations in Fig. S3.

For the quality control of the data for migration we followed the approach described in Hetényi et al. (2015) and Singer et al. (2017). This involved a first round of criteria inspecting the original Z-N-E component records for two signal-to-noise ratio metrics (peak amplitude to background amplitude and to background rms), and (dis)similarity of waveforms at various stations across the array for each event. A second round of criteria verifies the location and amplitude of the most prominent peak of the computed radial (R component) receiver functions in the considered frequency band. In addition, for this phase, a visual control of receiver functions, station by station and ordered by back-azimuth, allowed to discard a small number of suspicious traces as well as station AAE33. As a result, 3537 traces are kept for migration. This is only about one quarter of our entire dataset, but our previous experience makes us prefer quality over quantity (e.g., ca. top-5% of data used in Nábělek et al., 2009).

Time-to-depth migration is performed using the CCP approach (e.g., Zhu, 2000). We incorporate the true elevation of stations, perform ray-tracing at 0.5 km depth-intervals, and create the migrated image with 1 km lateral bin size. This approach relocates the converted-wave amplitudes of the observed RF along the theoretical ray-path at depth. Following a pre-stack migration, coherent high-amplitude signals will connect to primary interfaces. A straightforward but often neglected step is to take advantage of the multiples as well. For this, an artificial velocity model is created to bring the later (deeper-lying) multiples to

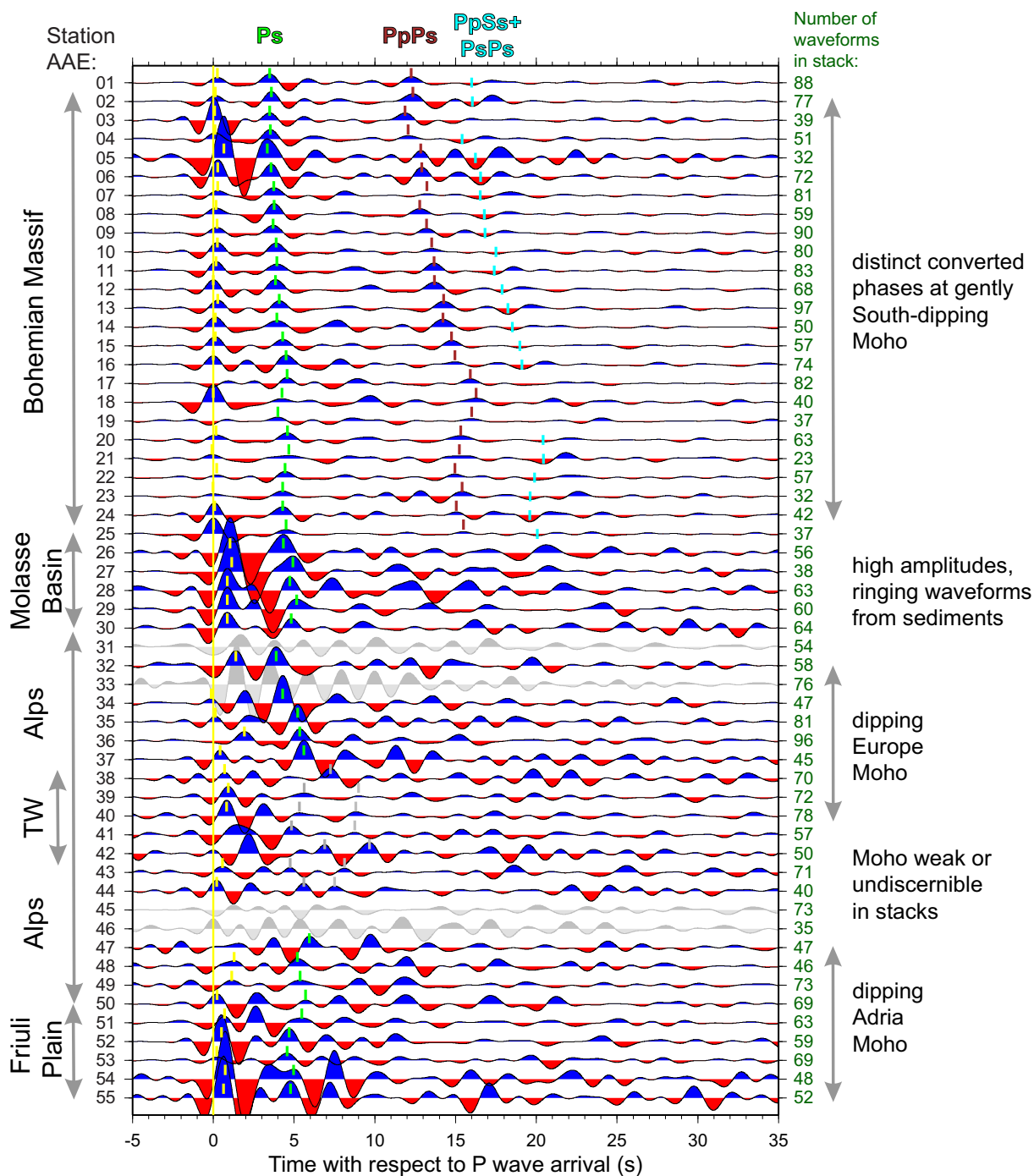


Fig. 3. P-to-S receiver-function station stacks shown for the 55 EASI stations, filtered in the 0.125–1 Hz range, calculated in the L-Q-T system and here showing the radial (Q) component, stacked using 6.4 s^2 slowness. See figure for description, grey traces correspond to ringing waveforms with questionable usefulness. The marked picks are used to construct part of Fig. 4. Abbreviations as in the main manuscript text.

the expected Moho depth. If the original velocity model's v_p/v_s was appropriate, the migrated image of the multiple phases matches the Ps phase migration image. This can be used in the reverse way: if the images resulting from migrating the Ps phase and multiples do not match, the v_p/v_s of the original model has to be updated accordingly. For details we refer to Hetényi (2007). We employ this approach using the *EPcrust* P- and S-wave velocity model (Molinari and Morelli, 2011) for migration of the Ps and PpPs phases, and calculate the final Moho depth and average v_p/v_s profile (see Section 4.3). Results of this approach are discussed in Section 4.3 and shown in Figs. 5 and 6, and the Moho depth information is provided in the Supplementary data file.

3.3.4. Dipping interfaces

The ability of RFs to image dipping interfaces is limited. Single-station analyses, either by displaying traces as a function of back-azimuth, or via harmonic decomposition (see Section 3.3.1) give useful first-order information about dip angles and orientations. Migration techniques give much better spatial location of converters. However, they may lack the continuity between different conversion points, especially if large horizontal smoothing is applied. Nevertheless, the change in migrated images as a function of illumination (back-azimuth of incoming rays) is a powerful tool to identify which of the discontinuities represent dipping interfaces ($< 40^\circ$). Teleseismic rays

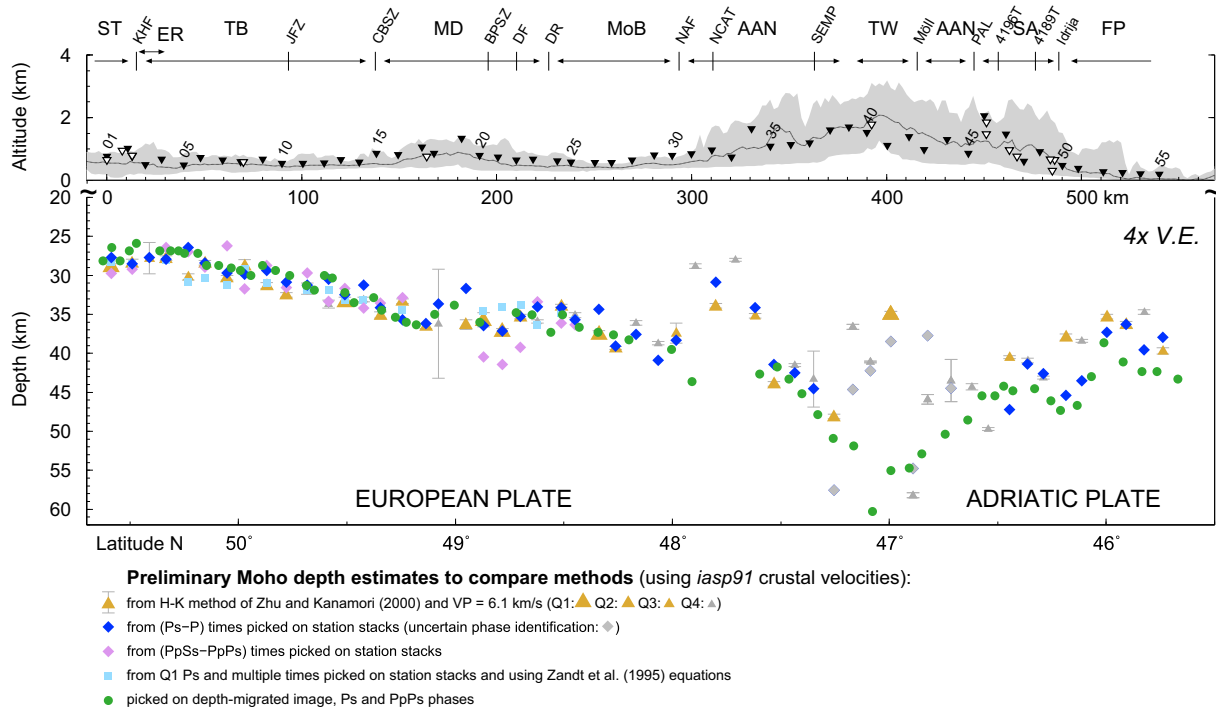


Fig. 4. Comparison of Moho depth estimates obtained with various approaches based on receiver functions, as described in the text, and using the simple *iasp91* velocity model. This figure serves for comparison of methods, and is not the Moho determined in this study along the whole swath (see Figs. 6 and 8). Note the four-fold vertical exaggeration. Q1–Q4 refer to various quality determinations. Top panel shows the topographic profile (grey shaded between minimum and maximum, average shown with black line) and EASI stations (last two characters shown for some). Abbreviations in addition to those on Fig. 1: ER – Eger Rift, DR – Danube River, MoB – Molasse basin, AAN – Austroalpine nappes, TW – Tauern Window, SA – Southern Alps, FP – Friuli Plain. 4196T and 4189T are minor faults.

undergo mode conversion at an interface only if they arrive with incidence angles clearly different from zero relative to the interface. Therefore, rays coming from the down-dip direction will cause large amplitude converted phases, while those arriving from the up-dip direction (nearly perpendicularly) will cause weak or no conversions. For illustration we refer to Hetényi (2007). This approach is exploited in the results described in Section 4.3 and shows in Fig. 5d, e.

3.3.5. RF waveform inversion

The main challenge of this study is to focus on the root of the Eastern Alps, beneath the Tauern Window, with the aim to characterize the S-wave velocity structure with depth. To this end we employ the Neighbourhood Algorithm (NA) technique and software (Sambridge, 1999), which has been applied to the non-linear RF problem on numerous occasions (e.g., Hetényi and Bus, 2007; Hetényi et al., 2011a). We apply the method to the identical RF dataset that was used for migration.

The NA is a stochastic inversion scheme that samples the better fitting part of the parameter space in an adaptive way, and avoids local minima in general. It inverts for the thickness, v_p and v_p/v_s of all layers entered in the model, and sets a linear velocity gradient in each layer. The layers are isotropic and are separated by flat discontinuities. In our study inversions have been run over 100 iterations with 100 velocity-models in each, of which the best 80 results defined the parameter space to be resampled in the subsequent iteration. This is how we carry out the exploratory search of the parameter space, which we initially define broad enough to be able to image a thick crust and variations of crustal velocities. The results are evaluated according to how well synthetics reproduce observed RFs filtered up to 0.55 Hz, compared using the L2 norm. The later part of the waveform stacks in the TW did not carry peaks with significant amplitudes to influence the inversion (Fig. 7). Therefore, we focused in the inversion on the first 10 s of the RF, thus excluding the Moho multiples obscured by the noise. In the

evaluation of the results, we considered the single best velocity model, as well as the best 1% of all results and their average. Inferences of this approach are discussed in Section 4.4 and shown in Fig. 7.

4. Results from top to bottom

4.1. Shallow structure

The shallow structure along the EASI profile has been investigated using harmonic analysis of data at each station. Fig. 2 shows the observed structure, with prominent signal in the first 15 km depth beneath the Eastern Alps. The local minima and maxima in the constant component of RFs, highlighted with circles in Fig. 2a, show deepening of the signal towards the centre of the orogen. These extremes are reported as rectangles on the $k = 1$ component picture (Fig. 2b), which highlights the occurrence of non-horizontal structural features (such as dipping interfaces or anisotropy with tilted symmetry axis). The deepening towards the orogen centre coincides with the deep-reaching faults of the geological profile at this longitude (Egger et al., 1999). On the northern side of the Alps, the negative converters (marked by red rectangles in Fig. 2b) start from the base of the Molasse basin and deepen southwards in a shape that recalls that of the Sub-Tauern Ramp observed on the TRANSALP profile. The positive converters (blue rectangles) follow deeper the negative converters in a sub-parallel way and reach ca. 15 km depth. This phase can also be identified on station stacks (Fig. 3). On the southern side of the Alps, the positive (blue) converters deepen by up-and-down jumps from one station to another. Such a finding indicates that stations along the West and East lines of the EASI profile, detect the signals at depths which differ by up to 5 km. This clearly points to strong lateral variations in the shallow structure within the width of the swath (ca. 12 km) and suggests the eastward shallowing of the converter responsible for the positive signal.

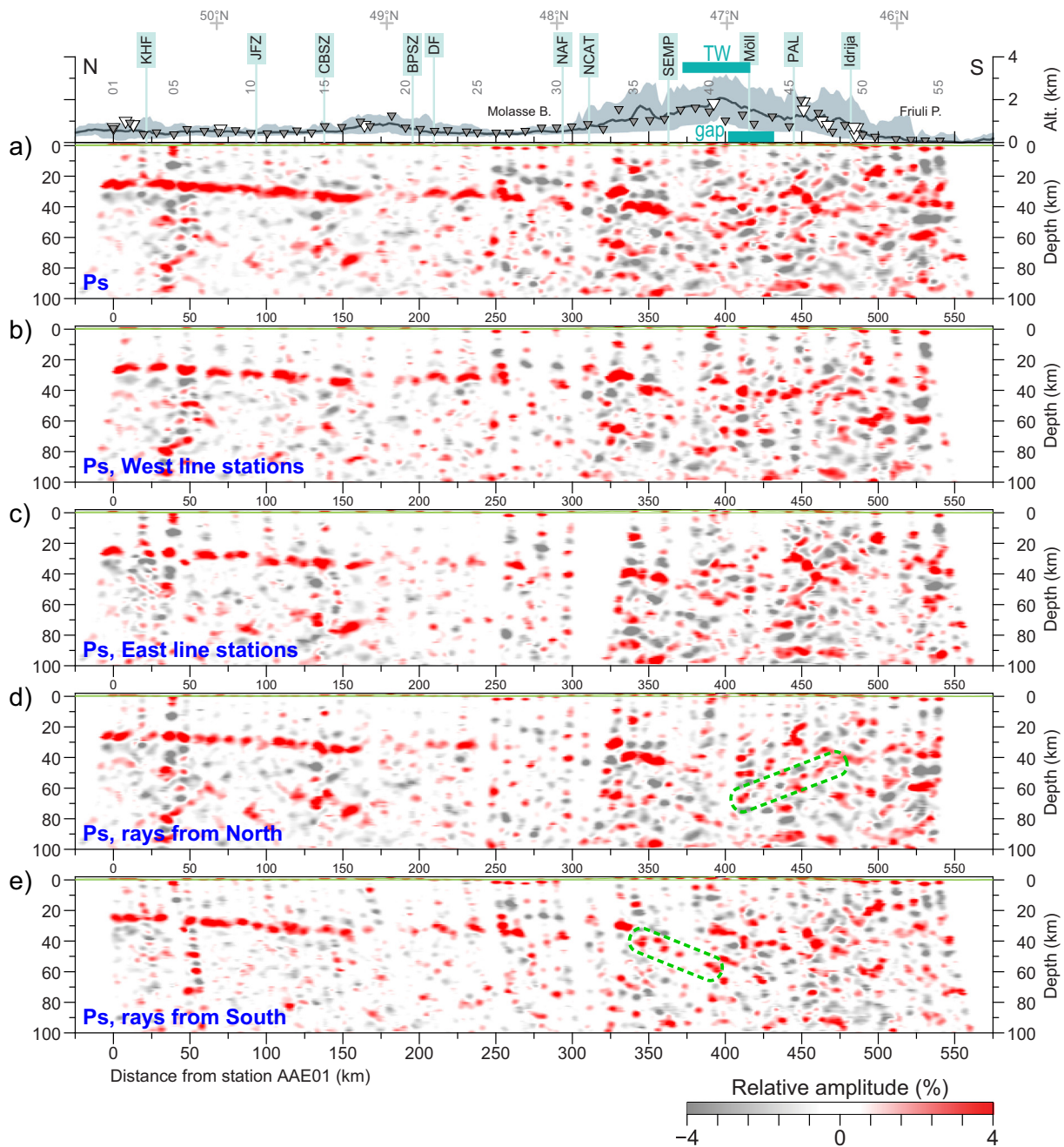


Fig. 5. Migrated receiver-function profiles using data from 55 EASI and 14 additional stations as well as the *EPcrust* velocity model (see text for further technical details). The five panels from top to bottom show: image using all rays (a), image using West (b) and East (c) line stations to show lateral variability. Images using rays coming from the north (d) resp. south (e) enhance northward resp. southward dipping interfaces, contoured with green dashed lines for the suggested Moho in the critical distance range beneath the orogen. Topography and geological references as on previous figures. TW – Tauern Window, gap – Moho gap (Spada et al., 2013). (For interpretation of the references to colour in this figure legend, the reader is referred to the web version of this article.)

4.2. Moho depth estimate comparisons

A first insight into along-profile variations is already visible on station stacks (Fig. 3). They show differences in structure of the crust accompanied by changes of Moho depth crossing the geological units from the north to the south. Although the instrumentation and installation types have varied little along the profile, there are distinct differences in the recorded signals. Clear conversions and multiples from the Moho appear in the Bohemian Massif, but reverberations at the shallow sedimentary layers of the Molasse Basin and Friuli Plain mask the Moho conversions. Beneath the Alps, a complex intra-crustal structure and Moho dip make measuring phase arrivals in station stacks

difficult, partly because of azimuthal dependence. Identification of the Moho-converted phases beneath the Tauern Window (ca. stations AAE39–AAE46) cannot even be speculated.

To compare the Moho depth estimates from various methods and to judge their reliability, we take advantage of the approaches described above (Sections 3.3.2 and 3.3.3). Fig. 4 summarizes all four estimates based on single-station approaches (including error-bars and grey shading in case of poor quality and uncertain phase identification), as well as the Moho depth picks from depth migrated RF. All these approaches use the same, 1-D velocity model *iasp91*. The northern half of the profile shows a generally good match between the various estimates, within a range of ca. ± 2 km. The Moho is 26–30 km thick

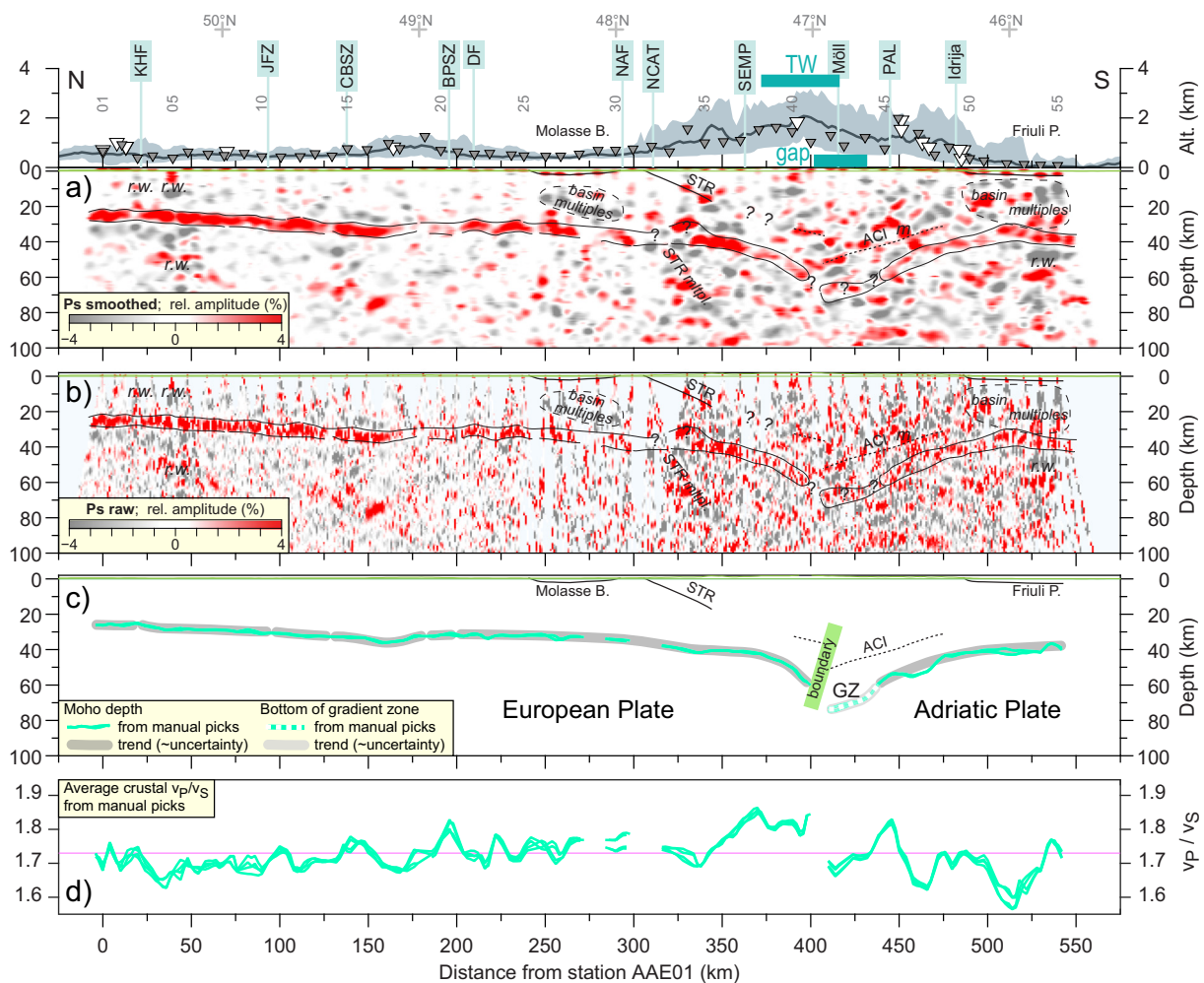


Fig. 6. (a) Interpreted migrated smoothed receiver-function profile showing structures and artefacts. The Moho Ps conversion is contoured with a thin black line. STR – Sub-Tauern Ramp, ACI – Adriatic Crustal Interface, r.w. – ringing waveform, m – multiple of a shallower converter. (b) Same as (a), but on the raw RF migration image (no smoothing, see also Fig. S4). (c) Key structural elements of the migrated profile taken for the interpretation. The thin green lines are Moho depths computed on migrated Ps and PpPs phases. GZ – gradient zone, with its bottom marked in a white-dotted line (see text). Interfaces in the orogenic root are only imaged by RF with migration (see Fig. 4). The sub-vertical green band is the proposed plate boundary at middle and lower crustal depths (d) Average crustal v_p/v_s ratio deduced from Ps- and PpPs-converted phase images simultaneously with Moho depth; short-wavelength variations denote processing-related uncertainties on the order of ± 0.05 . Pink line at 1.73 is shown for reference. Moho depth differences with respect to Fig. 4 are explained in the text. (For interpretation of the references to colour in this figure legend, the reader is referred to the web version of this article.)

beneath the northern end of the profile in the Bohemian Massif (shallowest at the Eger Rift) and deepens gradually towards the south. At about 160 km distance, the Moho deepening stops, and the various methods give a more diffuse pattern of Moho depth-estimate at the edge of the BM, near the BPSZ. The Moho, in general, continues to deepen to the south beneath the Molasse Basin, until an area of inconsistent results near the NAF and NCAT. Further south, there is a large variability of values beneath the Alps and the Friuli Plain, with many approaches unable to provide any reliable Moho depth estimate. Yet, the clear, relatively steep northward deepening of Adria can be ascertained.

It seems clear from our previous knowledge that in case of relatively simple crustal structure, such as in the Bohemian Massif, all methods provide similar estimates, which one can fine-tune with further analysis such as RF inversion for shear-wave velocity variation with depth, and joint inversion with other type of data. We also consider that Moho depth results are more reliable in the BM. However, in the thick and complex Alpine domain the single-station methods meet their limitations and can yield misleading results. Therefore, we focus our analysis on migrated RF profiles that relocate the wave-converting interface elements to their position at depth. Due to the crossing rays between neighbouring stations (Fig. S4), the migrated RF profiles provide a more

reliable, continuous image of the crust. Still, the reliability of Moho depth estimates is lower beneath the Alps due to reverberations and structural complexities.

4.3. Moho geometry

The most coherent picture of the Moho is drawn following pre-stack depth migration of P-to-S RFs. This is done using the regionally derived *EPcrust* P- and S-wave velocity model (Molinari and Morelli, 2011), the only one covering our entire study area. We show both the raw, not smoothed migration in Figs. S4 and 6b and discuss below the slightly smoothed RF images (Fig. 5). In general, uncertainties exceeding 5 km may arise from the choice of the velocity model. However, as we take advantage of a regionally derived v_p and v_s model and use both direct and multiple converted phases, we estimate the final Moho uncertainty is 2–3 km for the more simple, isotropic crust in the northern part of the profile, while larger uncertainties may exist beneath complex structures, like below the sedimentary basins and the TW.

The migration of all selected data shows features similar to that described above, with a deepening of the Moho towards the orogen centre, small interruptions in the BM and a generally complex structure

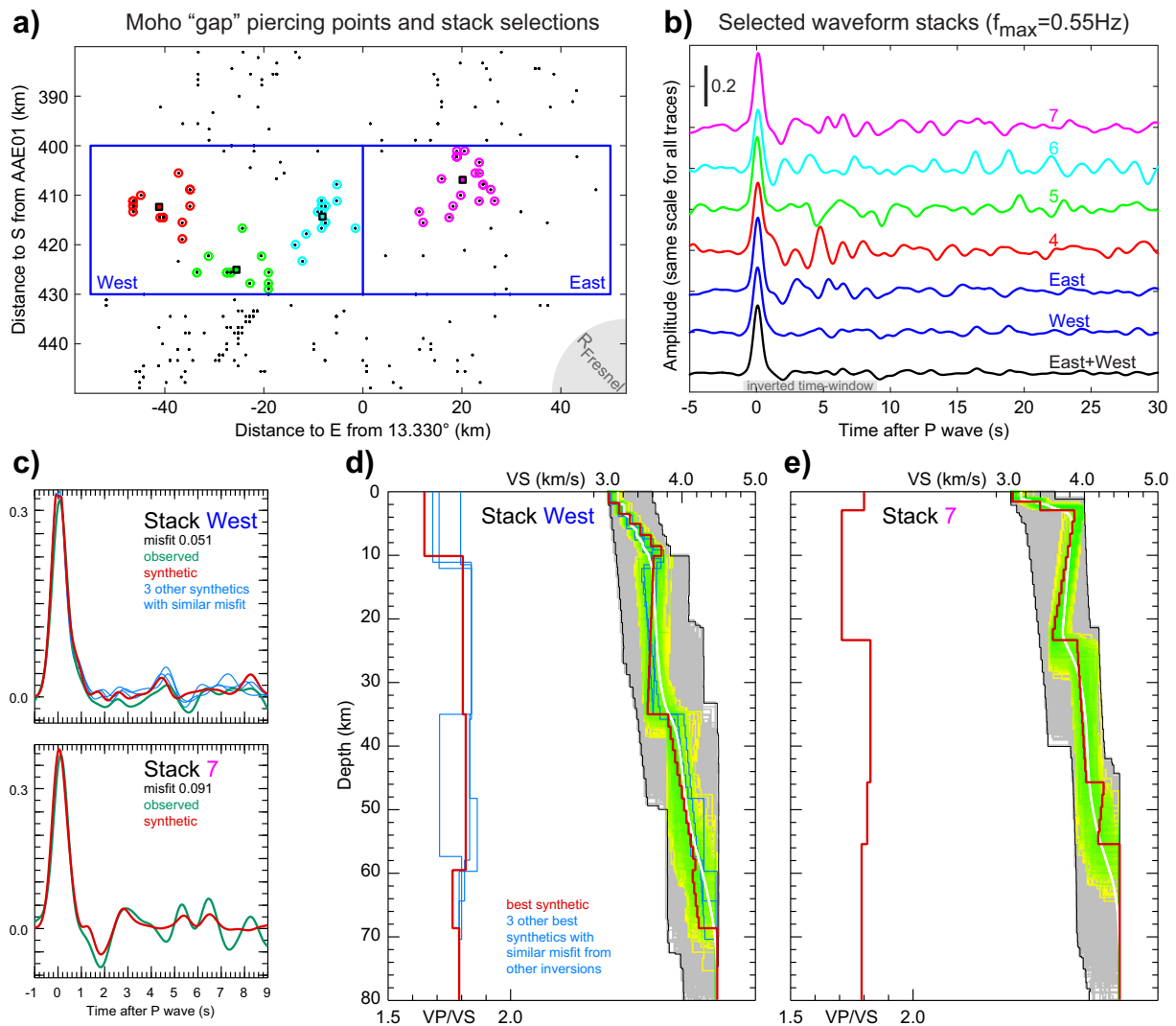


Fig. 7. Receiver-function waveforms and inversion results in the Tauern Window “Moho gap” area. (a) Geographic distribution of pierce points at 60 km depth and groupings. (b) Waveform stacks of receiver functions grouped as shown on the map; note the strong variability and lack of clear Moho Ps conversion at most stacks. (c) Waveform fits and (d) 1D velocity-model inversion results for two selected groups; note the lack of a clear velocity jump at Moho depths. The same data is used here as for migration, but at lower frequencies (0.55 Hz).

beneath the Eastern Alps. The Moho itself is not always easy to pick from the Ps phase. Therefore, we also relied on the migration of the PpPs phase (Fig. S4) for calculation of final Moho depth and average crustal v_p/v_s . Data from the additional 14 stations included in the migration proved to be critically important to identify the Moho of the Adriatic plate.

Interesting details emerge when the EASI swath and surrounding stations data are separated to western and eastern parts (Fig. 5b, c). Some of the tectonic terrain boundaries in the BM emerge more distinctly. We also identify clear variations of Moho depth (and depth of other conversions) laterally, despite the relatively short (12 km) west-east separation of the two EASI lines. This means that there are evident, strong variations of the crustal structure in the dimension perpendicular to the profile. This is an important warning for linear arrays across complex regions which may image structures but may fail at mapping several kilometre variations in depth along their strikes.

Another aspect of the results appears when only northern or southern back-azimuth arrivals are used for imaging (Fig. 5d, e). This polarized view of the crustal part of the lithosphere highlights dipping interfaces, as described above. The northern rays clearly delineate the north-dipping Moho beneath the Southern Alps (440–500 km distance), while the southern arrivals confirm several south-dipping converters in

the orogen (340–400 km distance). However, there is no strongly polarized pattern (major difference in amplitudes and connection of converters) observed around the Moho and the lower crust, as in the case of Tibet (Hetényi, 2007; Nábělek et al., 2009). The Moho signal is faint in between the identified, oppositely and convergently dipping Moho segments, just beneath the southern edge of the Tauern Window. This coincides with the Moho gap described in Section 2.3 with the lack of conversions/reflections in other analyses. The nature of this zone is further investigated in Section 4.4.

The migrated images focusing on the crustal structure contain, by their nature, multiples of shallower interfaces. These reverberations are very clearly visible beneath the Eger Rift (station AAE05), the Molasse Basin and the Friuli Plain, as well as within the Alps (e.g., at 450 km distance). The most important of these artefacts were identified (Fig. 6a, b) and discarded for the interpretation (Fig. 6c) where the final Moho depth combining Ps and PpPs phase information is shown. Note that the (sometimes significant) Moho depth differences between Figs. 5 and 6 and Fig. 4 are due to the usage of different velocity models: the 1-D *iasp91* in the single station methods, in an initial RF migration and their comparison (Fig. 4), whereas the regional 3-D velocity model *EPcrust* was used for the final RF migration (Figs. 5 and 6). Though the depth extent of the crustal root depends on the velocity model used for

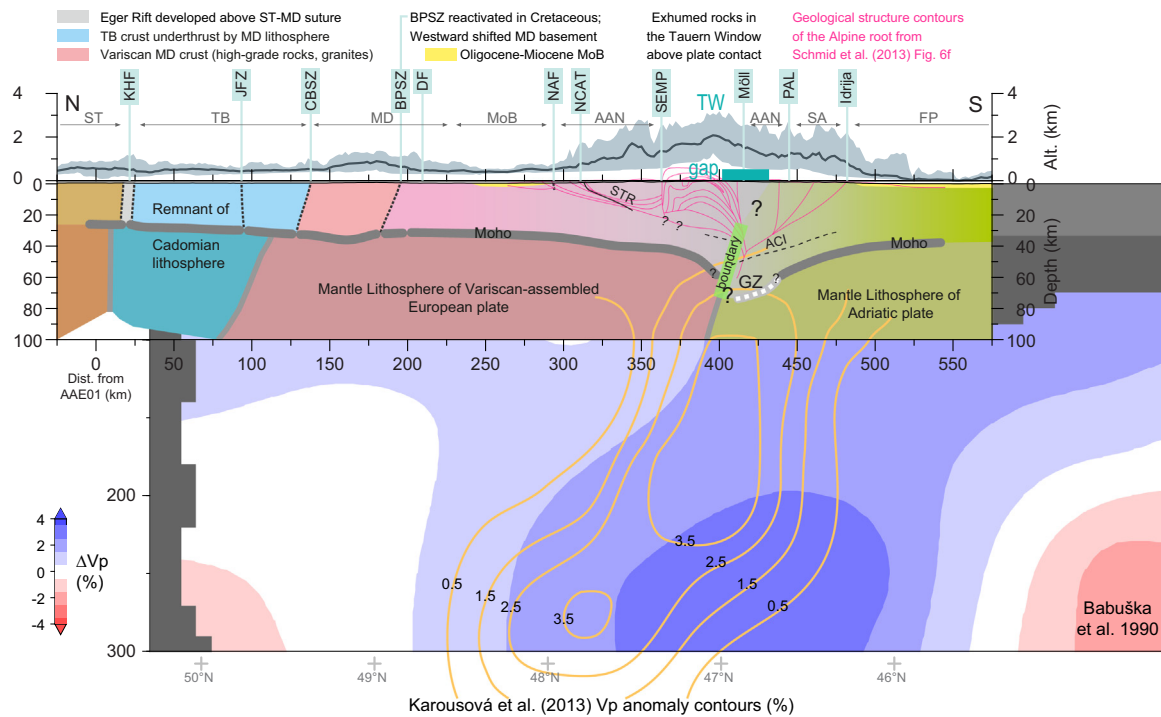


Fig. 8. Interpretation of the EASI receiver-function results (this study) complemented using previous geological and geophysical knowledge. The sub-vertical green band is the proposed plate boundary at middle and lower crustal depths. GZ – gradient zone, with white-dotted line as bottom. See Fig. 1 and text for full description. The pink lines contour the geological structure as sketched by Schmid et al. (2013), located using the surface trace of the SEMP fault. The colour-plotted P-wave tomography result (1.5° resolution) is redrawn from Babuška et al. (1990). The contours of Karousová et al. (2013)'s P-wave tomography are shown for comparison (40 km resolution). Abbreviations as throughout the manuscript. (For interpretation of the references to colour in this figure legend, the reader is referred to the web version of this article.)

the RF migration, the shapes remain similar. Moreover, including more data from additional stations in the region in the final dataset allowed confident picking of the Adriatic Moho.

The average crustal v_p/v_s along the EASI transect is shown in Fig. 6d. Short wavelength variations are due to the processing of this dataset (e.g., sampling Ps and PpPs migrated images at different distances and interpolating before v_p/v_s calculation). The long wavelength trend shows an increase of v_p/v_s from ca. 1.7 in the northern part of the BM to ca. 1.75 at the Molasse Basin, and then to ca. 1.8 in the Northern Alps. For the Adria plate the value is 1.70–1.73, on average, with short-wavelength disturbances preventing a more detailed analysis. Nevertheless, the difference in average crustal v_p/v_s beneath the Alps above the Adriatic and European plates is evident, and is not an artefact of the assumptions made during our approach.

4.4. Focus on the Eastern Alpine root

As described above, the orogenic root beneath the southern edge of the Tauern Window lacks a strong Moho signal on migrated P-to-S RF images (Figs. 5, 6) as well as on station stacks (Fig. 3). However, it is not a completely transparent Moho gap: yet, a northward dipping interface can be ascertained (Figs. 5, 6a, b). Therefore, we attempt to better characterize the nature of the crustal root by RF waveform inversion. To do so, we gather a bundle of teleseismic rays sampling the Alpine root at 60 km depth between 400 and 430 km distance along the EASI profile. We stack various groups of waveforms, both over the entire zone, western and eastern parts separately, as well as several subsets covering areas comparable to the Fresnel zone (Fig. 7a, b).

From the group stacks it is clear that the structure of the root in the Eastern Alps is complex and spatially highly variable, as the general shape of waveforms varies a lot. Most of the stacks lack a prominent Ps phase, which points towards broad velocity gradients with depth, instead of sharp discontinuities. An attempt to modify that by including

additional layers in the inversion did not change the gradient character of the resulting velocity profiles.

As a quantitative test we perform inversions to obtain v_s as a function of depth for the “Stack West” and for “Stack 7”. Best fit waveforms and corresponding velocity models are shown in Fig. 7c, d and e. For “Stack West”, the best synthetic and three other waveforms with similar misfit resemble the observed one in comparable ways, but miss some of the peaks. In the corresponding v_s profiles, all these and other well-fit models show no or very small (ca. 0.2 km/s) velocity increases. However, the suspected Moho depth range is very large, between 50 and 70 km depth. The most credible velocity jump is located at ca. 35–39 km depth (also visible on migrated sections, especially for the “West line stations”, Fig. 5b). For “Stack 7”, the best fit model has 0.3 km/s increase at 56 km depth, but the group of best-fit solutions fails to highlight a single velocity increase associable with a Moho. The model reaches mantle velocities over a broad depth range (48–65 km).

All these observations suggest that the orogenic root is devoid of a sharp crust-mantle boundary (a proper Moho). It can be best described by a broad, up to ca. 20 km thick vertical velocity gradient zone, with distinct spatial variability, and with its base reaching ca. 70 km depth. Receiver functions are able to detect this broad vertical velocity gradient thanks to the inherently included low frequencies. On top of that, teleseismic rays illuminate the region from below and guarantee sampling across the entire gradient zone (GZ). This is coherent with the Moho gap proposed earlier, that was aimed to be imaged by higher frequency, locally generated waves reaching the Alpine root from above, and returning little or no signal from the upper part of the gradient zone. Neither of the approaches is able to detect eventual vertical boundaries that may be present in the complex structure of the orogenic root. Inversion of other waveform stacks shown in Fig. 7b point to the conclusions drawn from the two examples presented in detail.

5. Interpretation and discussion

The converging European and Adriatic plates create complex tectonics of the Alps, both at shallow depths of the crust and deeper in the mantle (lithosphere). The following sections and Fig. 8 provide an overview of the results from top to bottom of both the structural and the geodynamic interpretation.

5.1. Shallow structures

Both major sedimentary basins, the Molasse Basin (MoB) and the Friuli Plain (FP), are clearly imaged in our results. Moreover, multiples of converted waves mask some of the upper crustal structures (Fig. 6). The geographical boundaries of the imaged basins coincide with those known from geology. The likely complex northern front of the Alps is poorly imaged at shallow depth. Part of this is due to noisy data and lack of coverage due to eliminated traces. Furthermore, complicated shallow velocity structure due to some sediments underthrusting the northern front, as described on geological profiles (Egger et al., 1999), can contribute to this. The Sub-Tauern Ramp is only partly imaged too, but its position and dip fit observations from TRANSALP well and also the geological structure proposed by Schmid et al. (2013). The multiples related to the STR, however, partly overlap with the Moho signal between 300 and 335 km in-profile distance, causing a lack of clear Moho detection.

5.2. Crustal structure

The crust–mantle boundary is clearly identified along most of the profile, except for the northern Alpine front (see Section 4.2) and the Alpine root (see Section 4.4), where Moho detection is less clear. The shape of the Moho generally agrees with earlier estimates and seems to refine them (Fig. 9). Results of the pre-stack RF migration add new information on the base of the gradient zone in the crustal root of the Eastern Alps. Besides its mere identification, the Moho's appearance varies greatly. As a general observation, the variability of the Moho image with azimuth helps to highlight its dipping segments (Fig. 5d, e), however, its amplitude does not depend strongly on back-azimuth, as in the case of central Tibet. There, the back-azimuthally strengthening and disappearing signal was interpreted as macro-fabric related to the mechanical decoupling and shearing during underthrusting of the lower lithosphere (Hetényi, 2007; Nábělek et al., 2009). The absence of such anisotropy in the Eastern Alps indicates that they have experienced less or no such effect at the Moho level in the south-north direction. Yet, decoupling within the orogenic crust or at the Moho must have occurred in order to accommodate lateral eastward extrusion.

5.2.1. Bohemian Massif

The southward increase of crustal thickness beneath the Moldanubian part of the BM towards the Alps is not monotonous. Interruptions in the deepening relate to significant faults or sutures between individual crustal blocks of varying thicknesses or appearances (Fig. 8):

- locally lower amplitude and a change in dip at the shallowest point of the Moho beneath the Eger Rift, at the boundary between the ST and TB units of the crust;
- locally weaker amplitude at the CBSZ, separating the TB and the MD crustal units;
- weaker amplitudes and change of Moho shape north of the BPSZ and possibly DF.

These three observations strengthen the interpretation of mantle lithosphere domains (Babuška and Plomerová, 2013), in which boundaries of adjacent domains remain since Variscan and Cadomian times at the same or slightly shifted locations relative to crustal blocks. We note that some of the signal in our images, like minor Moho steps, may also come from lateral variations in structure or velocity within the east-west extent of the EASI swath. For example, the Moho high (Moho-depth minimum) at 160–200 km distance is distinct on the East line of the EASI transect, while conversions on the West line are weak (Fig. 5b, c). Such short wavelength differences show the high capability of RFs to identify lateral variations of structures. We rule out small-scale amplitude variations due to uneven data coverage being the primary cause of these observations, as data coverage is good (Fig. S4) and because these boundaries coincide with geological inferences such as tectonic units.

The general southward increasing trend in average crustal v_p/v_s in the BM (Fig. 6d) is not an artefact of poor velocity model or a too smooth Moho geometry, as a simply deeper Moho would result in lower v_p/v_s . Instead, this trend may correspond to a slightly increasing amount of mafic material in the crust or different evolution history of the currently adjacent crustal blocks.

5.2.2. Alps and Europe-Adria contact

The deep structure of the Alps along longitude 13–13.5°E is clearly bi-vergent (Figs. 6, 8). On the north side, the deepening of the European Moho ends on a shorter wavelength down-bending, which could indicate crustal buckling that is representative of mature collision stage (Burg et al., 2002), or downward dragging by the descending Adria plate. The south side appears to curve more broadly, suggesting flexural bending of the descending Adriatic lithosphere. A 30 km long less clearly imaged zone appears between the two, oppositely and convergently dipping Moho segments. The position and dip of the respective lower crusts is verified by the images drawn by rays arriving only from the north and south (Fig. 5d, e), as well as a ca. 70 km long segment of an interface that resembles the Adria Crustal Interface of the TRANSALP profile (Figs. 6, 8). On the European side, a short (ca. 20 km long) converter segment above the Moho could be either the deeper end of the STR, or another converter resembling a reflector imaged in TRANSALP. This reflector in TRANSALP has led to two different interpretations: the “Crocodile model” for Adriatic wedging and crustal imbrication and the “Lateral extrusion model” for a smoother, steeply dipping front of the Southern Alpine indenter.

Considering our images, a crocodile-type model, with a piece of Adria lower crust wedging into the European lithosphere, does not seem to be credible, and this for two reasons. First, around 400–410 km distance, there are three positive RF converters above each other, but

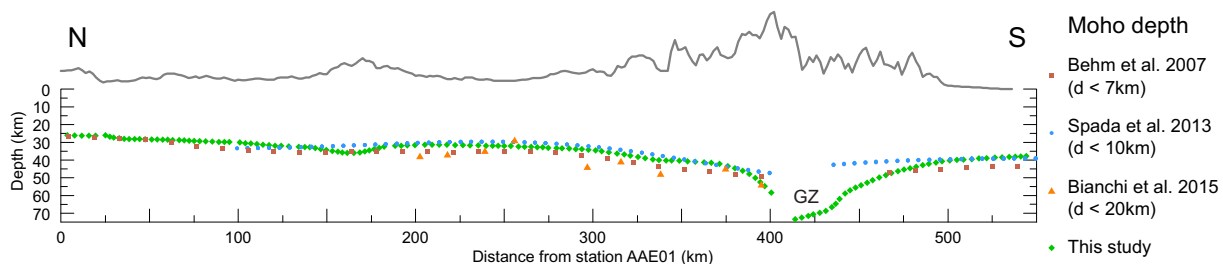


Fig. 9. Comparison of Moho depths along 13.3°E from various studies shown in the legend. The Moho depth values are taken within distance d of the profile in the respective studies. GZ – gradient zone as discussed in this study.

only two of them seem to be reasonable in a crocodile-model, considering a classical upper crust – lower crust – mantle velocities, unless these units of Europe and Adria have very different impedances. In other words, in a synthetic crocodile-type model only two interfaces would produce converted waves, and the third one that is observed in nature would remain unexplained. Second, from a rheological point of view, it seems unlikely that the lowermost crust or the uppermost mantle of either plate can be bent back and continue upwards. If there is a crocodile-type imbrication of the two lithospheres, it must be below the scale resolved by receiver functions, or the two lower crusts must have very different impedances to fit our images.

Instead, we propose the simplest acceptable solution for crustal architecture of the Eastern Alpine root: oppositely deepening interfaces for both European and Adriatic crusts, and a nearly vertical, yet north-dipping boundary zone at the contact of the two plates at ca. 30–70 km depth (see green band in Figs. 6 and 8). Such a broad boundary fits all our observations made by receiver functions and is also consistent with the deep detachment surface inferred from structural geology as shown in Fig. 8 (Schmid et al., 2013). The Periadriatic Line remains invisible to our seismic methods, as it also did in TRANSALP. The Adriatic Crustal Interface (ACI), imaged and interpreted by TRANSALP as Adriatic upper–lower crust boundary, follows roughly the Adriatic Moho (with some northward thickening of the lower crust) and is deeper than the deepest structural boundary proposed from geological observations (Fig. 8, Schmid et al., 2013). The seismologically imaged STR coincides with geological inferences down to 20 km depth, and may or may not connect with the imaged deeper short converter that abuts the proposed plate boundary zone at ca. 400 km distance along profile. The steeply north-dipping, ca. 30 km broad boundary zone in the crust proposed here fits very well the deeper lithospheric structure inferred by a regional high-resolution upper mantle tomography study (Karousová et al., 2013; Fig. 8).

Unfortunately, the ACI cannot be followed to the south due to interference with basin multiples. However, the lithospheric configuration (e.g., Babuška et al., 1990) and plate relation proposed here identifies Adria as the subducting plate. Therefore, the setting of the devastating M6.5–7.0 earthquakes discussed above (Fig. 1) qualifies that they were megathrust earthquakes, with the Friuli Plain being the Mio-Pliocene foreland basin of the Eastern Alps.

5.2.3. The crustal root of the Eastern Alps

One of the main motivations for EASI was to verify the existence of the Moho gap beneath the Tauern Window, described in Section 2.3. Our images testify that the contact between the European and Adriatic Moho remains a difficult target. This is partly due to short-wavelength lateral variations (Fig. 5b, c). The East line image shows no signal, coherent with the Moho gap detected earlier, whereas the West line has a weak signal along the 30 km long segment in question. We associate this deeper interface with the base of the gradient zone, which clearly represents a new result compared to earlier studies (Fig. 9). Our targeted RF inversion to retrieve v_s structure with depth has revealed a broad, up to 20 km-thick velocity gradient between crustal and mantle velocities beneath the TW (Fig. 7).

This broad gradient zone explains why active seismic methods imaging this area have detected a Moho gap, and why RFs, sensitive to lower frequencies and sampling from below, recover a weak signal. We imagine the orogenic root as a zone of small-scale heterogeneities resulting from the collisional process of the middle and lower crust and the uppermost mantle. The shape of the Alpine root is convex downward, resembling a cup, which may also act as a sink for lower crust that may undergo high-pressure metamorphism (e.g., Schmid et al., 2013; Favaro et al., 2017). The deformation of this root depends very much on temperature and rheology, but this sink enhances localization of the orogenic root (see Hetényi et al., 2011b).

This broad vertical GZ of velocities and density also explains why such an extremely deep Moho signal is plausible in light of earlier

studies, i.e. estimates of crustal thickness and observed gravity anomalies (e.g., Ebbing et al., 2006). Much of this dense crustal root is above the lowermost seismic converter, but already has high densities approaching those of the mantle. Due to their small density contrast with the mantle, their contribution to negative Bouguer anomalies at the core of the Alps is very small. The situation is similar to that of the lower crust of India beneath southern Tibet, where the major density jump is at a shallower depth than the major velocity jump, and corresponds to eclogite-facies metamorphism of the lower crust (Hetényi et al., 2007). The unusual thickness of the lower crust in the Eastern Alpine root was proposed to stem from the accretion of two subduction-accretion episodes (Handy et al., 2015). For a quantitative evaluation, further analysis of our proposed crustal configuration with density modelling and gravity anomaly data is required.

5.2.4. Comparison to TRANSALP

The comparison of the EASI results with those from TRANSALP, located only ca. 100 km further west, reveals both similarities and differences. The intra-crustal features such as the Sub-Tauern Ramp and the ACI are comparable, though the STR reaches the surface further north along the EASI profile, where the Inntal fault merges with the NCAT (Fig. 1). The shape of the ACI and the general shape of Adriatic lower crust is similar to the result from TRANSALP (see Fig. 6 of Castellarin et al., 2003; and Fig. 5 of Lüschen et al., 2004). However, the sub-Dolomite ramp is not identified in EASI (Fig. 6), yet there must be a thrust fault that separates the Neogene orogenic wedge in the Southern Alps from the downgoing basement (Fig. 8).

The largest difference in the results of the two experiments is the shape of Adriatic indenter as seen in a N-S cross section: it is sub-horizontal in the TRANSALP section, but downbending in the EASI section. The comparison is difficult as TRANSALP had very few broadband seismometers (J. Kummerow, pers. comm.). However, assuming the TRANSALP images are credible, the shape of the Adria Moho is closely related to the presence or absence of the downgoing slab (i.e., EASI located above the N-dipping Eastern Alpine slab, TRANSALP located in a gap between the Central and Eastern Alpine slabs). Finally, the absolute depths of converters in TRANSALP are shallower than in EASI. The differences may be caused by the fact that the authors used a relatively old macro-velocity model to migrate at depth.

In our interpretation, the EASI experiment images structures that formed during Neogene indentation of the Adriatic microplate. These structures are compatible with the notion of lateral orogenic extrusion, but we emphasize that they do not represent the deep structures of the TRANSALP section, which formed during an earlier, probably Paleogene stage of the collision.

5.3. Deep lithospheric structure

The broad boundary zone in the lower part of the thickened crust that dips to the north at a high angle, together with the deeper-reaching Adria Moho beneath the Tauern Window, suggests that the Adriatic plate penetrates further down (Fig. 8). The general dip of the boundary zone is coherent with the dip of the velocity anomaly in the upper mantle imaged by teleseismic tomography (Babuška et al., 1990; Karousová et al., 2013), resolved by different datasets and with different spatial resolution along the same longitude (Fig. 8). Putting together tomography and receiver functions, it seems that the Eastern Alpine slab is attached to the Adria microplate, and that the subduction of Adria filled the void following tearing and break-off (von Blanckenburg and Davies, 1995) of the formerly southward subducting European plate (e.g. Handy et al., 2015). Though details of the plate subductions are unknown, the complex geometry is imprinted in the triangular shape of the depth sections of the Eastern Alpine lithosphere root (e.g., Plomerová and Babuška, 2010), in contrast to the shape of the single, though bent, subduction of the European plate beneath the Adriatic plate in the Western Alps.

Deep lithosphere studies in the Bohemian Massif that have exploited data from several passive experiments in the past and included seismic anisotropy, derived a general model of lower continental lithosphere as an amalgamation of several domains with different thickness and seismic fabrics. The domains often have their equivalents in the crustal blocks, both being separated by faults and deep sutures whose crustal and mantle parts used to be disconnected (e.g., Babuška and Plomerová, 2013). Our images showing Moho offsets strengthen these earlier findings and allow us to conclude on the comprehensive lithospheric scale cross section along longitudes 13–13.5°E presented in Fig. 8.

6. Conclusions

The EASI experiment aimed at shedding light on the crustal structure of the Eastern Alps and adjacent tectonic units. In this paper we accomplish that by using various methodologies based on teleseismic P-to-S converted waves and emphasizing the validity and limitation of individual methods.

The signature of the near-surface geology is well-identified in the EASI profiles. Both the sedimentary basins and the dipping or/and anisotropic layers in the upper crust are consistent with structures in geological cross-sections.

On a crustal scale, both the European and the Adriatic Moho deepen towards the Alpine orogen. On the European side, the disruption of the deepening of the Moho beneath the Bohemian Massif is related to first-order lithospheric block boundaries inherited from the Variscan orogeny, often expressed as faults on the surface. These clear Moho steps speak for a block structure of the BM crust, instead of multi-layer approximations with continuous lateral velocity variations, as often suggested by controlled source seismology results.

While the crust of both the European and Adriatic plates thickens towards the orogen, the latter probably even beyond 60 km depth, their contact at depth, located south and beneath the central part of the Tauern Window, is a challenge for direct imaging. This zone coincides with the Moho gap previously suggested from active seismic imaging. Whereas high-frequency crustal phases of controlled-source seismology sense this zone from above, the same zone appears to contain some weak signal when illuminated by lower frequency teleseismic waves crossing it from below. Converted-waveform inversion reveals a broad, up to 20 km thick zone of low velocity-gradient at the root of the Alpine crust, with its base at ca. 70 km depth. Further insights into this zone are not possible with our approach as the scale of heterogeneities is below resolution of the applied waves. Nevertheless, such a gradient zone can well act as a sink for lower crustal imbricates detached during subduction.

The deeper portion of our interpretative cross-section is based on our results combined with earlier seismic tomographic images. They draw a steeply northward dipping lithospheric slab in the upper mantle, which is connected to the Adria plate entering the collision zone from south. This configuration of the Eastern Alps confirms that the four strong earthquakes (magnitudes 6.5 to 7.0) since 1348 in the southern margin of the orogen occurred indeed in a megathrust setting.

Our experience with the EASI receiver-function study is that dense station spacing is only one prerequisite for successful crustal imaging. Other critical components are the duration of the deployment to acquire sufficient amount of data of sufficient quality, and at least some but preferably full coverage of geological structures in the dimension perpendicular to the profile. The already well-advanced AlpArray Seismic Network, although of lower spatial spacing, but of full 3D coverage and deployed for longer time, will provide additional insights into the crustal and upper mantle structure of the entire range of the European Alps.

Acknowledgments

We are most grateful for the seismic instrument pools and managers

to have provided the instruments deployed in EASI: ETH Zürich (SEG/SED), IG CAS Prague, U Vienna and INGV. We warmly acknowledge the full support of INGV in the fieldwork support throughout the experiment: Stefano Solarino, Aladino Govoni, Simone Salimbeni, Lucia Margheriti and Adriano Cavaliere. Likewise, we very much appreciate the work and support of the AlpArray-EASI Field Team from Prague (Helena Munzarová, Petr Jedlička, Josef Kotek), Vienna (Maria-Theresia Apoloner, Florian Fuchs, Patrick Ott, Ehsan Qorbani, Katalin Gribovszki, Peter Kolinsky, Peter Jordakiev, Hans Huber) and Zürich (Sacha Barman, Robert Tanner, Pascal Graf, Laura Ermert, Anne Obermann, Stefan Hiemer, Meysam Rezaeifar, Edith Korger, Ludwig Auer, Korbinian Sager, Irene Molinari, Paula Koelemeijer, Saulė Žukauskaitė, Marcus Herrmann, Sacha Winterberg). Special thanks to those who helped with the data management, archival and distribution: John Clinton, Roman Racine, Aladino Govoni and Luděk Vecsey. We are indebted to all who have hosted a seismological station in their house or on their property, including the University of Salzburg for the possibility of using Seppalm. Furthermore, we thank all national and regional observatories operating permanent stations from which we exploited data for making these available to the public. The EASI experiment and research would not have been possible without the financial support obtained for the teams at ETH Zürich (Institute of Geophysics and Swiss Seismological Service internal funding), at IG CAS Prague (Czech Academy of Sciences grant no. M100121201; Operational Programme Research, Development and Education project CzechGeo/EPOS-Sci, no. CZ.02.1.01/0.0/0.0/16_013/0001800) and at the University of Vienna (Austrian Academy of Science (ÖAW) funded project “Deep exploration of the Eastern Alps”; Förderung der Wissenschaftlichen Forschung (FWF) funded project “AlpArray Austria”, no. P26391). Furthermore, data acquisition from permanent observatories and development of the devices in Czech Republic was supported by the large research infrastructure project CzechGeo/EPOS (grants no. LM2010008 and LM2015079). We acknowledge the financial support of the Swiss National Science Foundation (grant PP00P2_157627). We warmly thank Edi Kissling for his overall contribution to the entire project, and also thank Jean-Pierre Burg for his suggestions. We are grateful to Vera Schulte-Pelkum and to Josip Stipčević for their constructive reviews, and Editor Ling Chen for her work.

Appendix A. Supplementary data

Supplementary data to this article can be found online at <https://doi.org/10.1016/j.tecto.2018.07.001>.

References

- Babuška, V., Plomerová, J., 1992. The lithosphere in central Europe - seismological and petrological aspects. *Tectonophysics* 207, 141–163.
- Babuška, V., Plomerová, J., 2013. Boundaries of mantle-lithosphere domains in the Bohemian Massif as extinct exhumation channels for high-pressure rocks. *Gondwana Res.* 23, 973–987. <https://doi.org/10.1016/j.gr.2012.07.005>.
- Babuška, V., Plomerová, J., Granet, M., 1990. The deep lithosphere in the Alps: a model inferred from P residuals. *Tectonophysics* 176, 137–165.
- Babuška, V., Fiala, J., Plomerová, J., 2010. Bottom to top lithosphere structure and evolution of western Eger Rift (central Europe). *Int. J. Earth Sci. (Geol. Rundsch.)* 99, 891–907. <https://doi.org/10.1007/s00531-009-0434-4>.
- Behm, M., Brückl, E., Chwatal, W., Thybo, H., 2007. Application of stacking and inversion techniques to three-dimensional wide-angle reflection and refraction seismic data of the Eastern Alps. *Geophys. J. Int.* 170, 275–298. <https://doi.org/10.1111/j.1365-246X.2007.03393.x>.
- Berkhout, A.J., 1977. Least square inverse filtering and wavelet deconvolution. *Geophysics* 42, 1369–1383.
- Bertrand, A., Rosenberg, C., Rabaute, A., Herman, F., Fügenschuh, B., 2017. Exhumation mechanisms of the Tauern Window (Eastern Alps) inferred from apatite and zircon fission track thermochronology. *Tectonics* 36, 207–228. <https://doi.org/10.1002/2016TC004133>.
- Bianchi, I., Bokelmann, G., 2014. Seismic signature of the Alpine indentation, evidence from the Eastern Alps. *J. Geodyn.* 82, 69–77. <https://doi.org/10.1016/j.jog.2014.07.005>.
- Bianchi, I., Park, J., Piana Agostinetti, N., Levin, V., 2010. Mapping seismic anisotropy

- using harmonic decomposition of receiver functions: an application to Northern Apennines, Italy. *J. Geophys. Res.* 115 (B12317). <https://doi.org/10.1029/2009JB007061>.
- Bianchi, I., Miller, M.S., Bokelmann, G., 2014. Insights on the upper mantle beneath the Eastern Alps. *Earth Planet. Sci. Lett.* 403, 199–209.
- Bianchi, I., Behm, M., Rumpfhuber, E.M., Bokelmann, G., 2015. A new seismic data set on the depth of the Moho in the Alps. *Pure Appl. Geophys.* 172, 295–308. <https://doi.org/10.1007/s00024-014-0953-1>.
- von Blanckenburg, F., Davies, J.H., 1995. Slab breakoff: a model for syn-collisional magmatism and tectonics in the Alps. *Tectonics* 14, 120–131. <https://doi.org/10.1029/94TC02051>.
- Bleibinhaus, F., Gebrande, H., 2006. Crustal structure of the Eastern Alps along the TRANSALP profile from wide-angle seismic tomography. *Tectonophysics* 414, 51–69. <https://doi.org/10.1016/j.tecto.2005.10.028>.
- Brückl, E., et al., 2007. Crustal structure due to collisional and escape tectonics in the Eastern Alps region based on profiles Alp01 and Alp02 from the ALP 2002 seismic experiment. *J. Geophys. Res.* 112, B06308. <https://doi.org/10.1029/2006JB004687>.
- Burg, J.-P., Sokoutis, D., Bonini, M., 2002. Model-inspired interpretation of seismic structures in the Central Alps: crustal wedging and buckling at mature stage of collision. *Geology* 30, 643–646.
- Castellarin, A., Cantelli, L., 2000. Neo-Alpine evolution of the Southern Alps. *J. Geodyn.* 30, 251–274.
- Castellarin, A., et al., 2003. The TRANSALP seismic profile and the CROP 1A sub-project. In: *Mem. Descr. Carta. Geol. d'It. LXIIpp.* 107–126.
- Chevrot, S., Girardin, N., 2000. On the detection and identification of converted and reflected phases from receiver functions. *Geophys. J. Int.* 141, 801–808. <https://doi.org/10.1046/j.1365-246X.2000.00139.x>.
- Crotwell, H.P., Owens, T.J., Ritsema, J., 1999. The TauP toolkit: flexible seismic travel-time and ray-path utilities. *Seismol. Res. Lett.* 70, 154–160.
- Dando, B.D.E., Stuart, G.W., Houseman, G.A., Hegedüs, E., Brückl, E., Radovanović, S., 2011. Teleseismic tomography of the mantle in the Carpathian–Pannonian region of central Europe. *Geophys. J. Int.* 186, 11–31. <https://doi.org/10.1111/j.1365-246X.2011.04998.x>.
- Dziewonski, A.M., Anderson, D.L., 1981. Preliminary reference Earth model. *Phys. Earth Plan. Int.* 25, 297–356.
- Ebbing, J., Braitenberg, C., Götz, H.-J., 2006. The lithospheric density structure of the Eastern Alps. *Tectonophysics* 414, 145–155. <https://doi.org/10.1016/j.tecto.2005.10.015>.
- egger, H., et al., 1999. *Geologische Übersichtskarte Der Republik Österreich 1:1,500,000*. Geologischen Bundesanstalt, Wien.
- Favaro, S., Handy, M.R., Scharf, A., Schuster, R., 2017. Changing patterns of exhumation and denudation in front of an advancing crustal indenter, Tauern Window (Eastern Alps). *Tectonics* 36, 1053–1071. <https://doi.org/10.1002/2016TC004448>.
- Frisch, W., Dunkl, I., Kuhlemann, J., 2000. Post-collisional orogen-parallel large-scale extension in the Eastern Alps. *Tectonophysics* 327, 239–265.
- Fügenschuh, B., Seward, D., Mancktelow, N., 1997. Exhumation in a convergent Orogen: the Western Tauern Window. *Terra Nova* 9, 213–217.
- Handy, M.R., Babist, J., Wagner, R., Rosenberg, C., Konrad-Schmolke, M., 2005. Decoupling and its relation to strain partitioning in continental lithosphere: insight from the Peri-Adriatic fault system (European Alps). In: Gapais, D., Brun, J.-P., Cobbold, P.R. (Eds.), *Deformation Mechanisms. Rheology and Tectonics: from Minerals to the Lithosphere*. Geol. Soc. London Spec. Publ. 243pp. 249–276.
- Handy, R., Schmid, S.M., Bousquet, R., Kissling, E., Bernoulli, D., 2010. Reconciling plate-tectonic reconstructions of Alpine Tethys with the geological-geophysical record of spreading and subduction in the Alps. *Earth Sci. Rev.* 102, 121–158.
- Handy, M.R., Ustaszewski, K., Kissling, E., 2015. Reconstructing the Alps–Carpathians–Dinarides as a key to understanding switches in subduction polarity, slab gaps and surface motion. *Int. J. Earth Sci.* 104, 1–26. <https://doi.org/10.1007/s00531-014-1060-3>.
- Hellfrich, G., Wookey, J., Bastow, I., 2013. *The Seismic Analysis Code. A Primer and User's Guide*. Cambridge University Press 9781107613195.
- Hetényi, G., 2007. Evolution of Deformation of the Himalayan Prism: From Imaging to Modelling. PhD Thesis. École Normale Supérieure – Université Paris-Sud XI (400 p). <http://tel.archives-ouvertes.fr/tel-00194619/en/>.
- Hetényi, G., Bus, Z., 2007. Shear wave velocity and crustal thickness in the Pannonian Basin from receiver function inversions at four permanent stations in Hungary. *J. Seismol.* 11, 405–414. <https://doi.org/10.1007/s10950-007-9060-4>.
- Hetényi, G., Cattin, R., Brunet, F., Vergne, J., Bollinger, L., Nábělek, J.L., Diamant, M., 2007. Density distribution of the India plate beneath the Tibetan Plateau: geophysical and petrological constraints on the kinetics of lower-crustal eclogitization. *Earth Planet. Sci. Lett.* 264, 226–244. <https://doi.org/10.1016/j.epsl.2007.09.036>.
- Hetényi, G., Stuart, G.W., Houseman, G.A., Horváth, F., Hegedüs, E., Brückl, E., 2009. Anomalous deep mantle transition zone below Central Europe: evidence of lithospheric instability. *Geophys. Res. Lett.* 36, L21307. <https://doi.org/10.1029/2009GL040171>.
- Hetényi, G., Vergne, J., Bollinger, L., Cattin, R., 2011a. Discontinuous low-velocity zone in southern Tibet questions the viability of channel flow model. In: Gloaguen, R., Ratschbacher, L. (Eds.), *Growth and Collapse of the Tibetan Plateau*. Vol. 353. pp. 99–108. Geol. Soc. London Spec. Publ. <https://doi.org/10.1144/SP353.6>.
- Hetényi, G., Godard, V., Cattin, R., Connolly, J.A.D., 2011b. Incorporating metamorphism in geodynamic models: the mass conservation problem. *Geophys. J. Int.* 186, 6–10. <https://doi.org/10.1111/j.1365-246X.2011.05052.x>.
- Hetényi, G., Ren, Y., Dando, B., Stuart, G.W., Hegedüs, E., Kovács, A.C., Houseman, G.A., 2015. Crustal structure of the Pannonian Basin: the AlCaPa and Tisza Terrains and the Mid-Hungarian Zone. *Tectonophysics* 646, 106–116. <https://doi.org/10.1016/j.tecto.2015.02.004>.
- Hetényi, G., et al., 2018. The AlpArray Seismic Network – a large-scale European experiment to image the Alpine orogen. *Surv. Geoph.* <https://doi.org/10.1007/s10712-018-9472-4>.
- ISC, 2015. On-line bulletin. <http://www.isc.ac.uk> (Internat. Seismol. Cent., Thatcham, United Kingdom).
- Karousová, H., Babuška, V., Plomerová, J., 2013. Upper-mantle structure beneath the southern Bohemian Massif and its surroundings imaged by high-resolution tomography. *Geophys. J. Int.* 194, 1203–1215. <https://doi.org/10.1093/gji/ggt159>.
- Kennett, B.L.N., Engdahl, E.R., Buland, R., 1995. Constraints on seismic velocities in the Earth from traveltimes. *Geophys. J. Int.* 122, 108–124.
- Kind, R., Yuan, X., 2011. Seismic receiver function technique. In: Gupta, H.K. (Ed.), *Encyclopaedia of Solid Earth Geophysics*. Encyclopaedia of Earth Sciences Series Springer, Dordrecht.
- Kind, R., Kosarev, G.L., Petersen, N.V., 1995. Receiver functions at the stations of the German Regional Seismic Network (GRSN). *Geophys. J. Int.* 121, 191–202.
- Kissling, E., Schmid, S.M., Lippitsch, R., Ansonje, J., Fügenschuh, B., 2006. Lithosphere structure and tectonic evolution of the Alpine arc: new evidence from high-resolution teleseismic tomography. In: Gee, D., Stephenson, R.A. (Eds.), *European Lithosphere Dynamics*. Vol. 32. pp. 129–145. Geol. Soc. London Memoirs.
- Kummerow, J., Kind, R., Oncken, O., Giese, P., Ryberg, T., Wylegalla, K., Scherbaum, F., TRANSALP Working Group, 2004. A natural and controlled source seismic profile through the Eastern Alps: TRANSALP. *Earth Planet. Sci. Lett.* 225, 115–129. <https://doi.org/10.1016/j.epsl.2004.05.040>.
- Lammerer, B., Gebrande, H., Lüschen, E., Veselá, P., 2008. A crustal-scale cross-section through the Tauern Window (eastern Alps) from geophysical and geological data. *London Geol. Soc. Spec. Publ.* 298, 219–229.
- Lenhardt, W.A., Švancara, J., Melichar, P., Pazdírková, J., Havří, J., Sýkorová, Z., 2007. Seismic activity of the Alpine-Carpathian-Bohemian Massif region with regard to geological and potential field data. *Geol. Carpathica* 58, 397–412.
- Ligorria, J.P., Ammon, C.J., 1999. Iterative deconvolution and receiver-function estimation. *Bull. Seismo. Soc. Am.* 89, 1395–1400.
- Lippitsch, R., Kissling, E., Ansonje, J., 2003. Upper mantle structure beneath the Alpine orogen from high-resolution teleseismic tomography. *J. Geophys. Res.* 108, 2376. <https://doi.org/10.1029/2002JB002016>.
- Liu, K.H., Gao, S.S., 2010. Spatial variations of crustal characteristics beneath the Hoggar swell, Algeria revealed by systematic analyses of receiver functions from a single seismic station. *Geochem. Geophys. Geosyst.* 11 (Q08011). <https://doi.org/10.1029/2010GC003091>.
- Lombardi, D., Braunmiller, J., Kissling, E., Giardini, D., 2009. Alpine mantle transition zone imaged by receiver functions. *Earth Planet. Sci. Lett.* 278, 163–174. <https://doi.org/10.1016/j.epsl.2008.11.029>.
- Lüschen, E., Lammerer, B., Gebrande, H., Millahn, K., TRANSALP Working Group, 2004. Orogenic structure of the Eastern Alps, Europe, from TRANSALP deep seismic reflection profiling. *Tectonophysics* 388, 85–102.
- Lüschen, E., Borrini, D., Gebrande, H., Lammerer, B., Millahn, K., Neubauer, F., Nicolich, R., TRANSALP Working Group, 2006. TRANSALP—deep crustal Vibroseis and explosive seismic profiling in the Eastern Alps. *Tectonophysics* 414, 9–38. <https://doi.org/10.1016/j.tecto.2005.10.014>.
- Matte, P., Maluski, H., Rajlich, P., Franke, W., 1990. Terrane boundaries in the Bohemian Massif: result of large-scale Variscan shearing. *Tectonophysics* 177, 151–170.
- Mattern, F., 2001. Permo-Silesian movements between Baltica and western Europe: tectonics and “basin families”. *Terra Nova* 13, 368–375. <https://doi.org/10.1046/j1365-3121.2001.00368.x>.
- Maupin, V., Park, J., 2007. Theory and observations: wave propagation in anisotropic media. In: Romanowicz, B., Dziewonski, A. (Eds.), *Seismology and the Structure of the Earth. Treatise on Geophysics*. Vol. 1. Elsevier, New York, pp. 289–321.
- Mitterbauer, U., Behm, M., Brückl, E., Lippitsch, R., Guterch, A., Keller, G.R., Koslovskaya, E., Rumpfhuber, E.M., Sumanovac, F., 2011. Shape and origin of the East-Alpine slab constrained by the ALPASS teleseismic model. *Tectonophysics* 510, 195–206.
- Mlčoch, B., Konopásek, J., 2010. Pre-late Carboniferous geology along the contact of the Saxothuringian and Teplá–Barrandian zones in the area covered by younger sediments and volcanics (western Bohemian Massif, Czech Republic). *J. Geosci.* 55, 81–94.
- Molinari, I., Morelli, A., 2011. EPcrust: a reference crustal model for the European Plate. *Geophys. J. Int.* 185, 352–364. <https://doi.org/10.1111/j.1365-246X.2011.04940.x>.
- Nábělek, J., Hetényi, G., Vergne, J., Sapkota, S., Kafle, B., Jiang, M., Su, H., Chen, J., Huang, B.S., Team, Hi-CLIMB, 2009. Underplating in the Himalaya–Tibet collision zone revealed by the Hi-CLIMB experiment. *Science* 325, 1371–1374. <https://doi.org/10.1126/science.1167719>.
- Ortner, H., Reiter, F., Brandner, R., 2006. Kinematics of the Inntal shear zone–sub-Tauern ramp fault system and the interpretation of the TRANSALP seismic section, Eastern Alps, Austria. *Tectonophysics* 414, 241–258.
- Park, J., Levin, V., 2000. Receiver functions from multiple-taper spectral correlation estimates. *Bull. Seismol. Soc. Am.* 90, 1507–1520.
- Plomerová, J., Babuška, V., 2010. Long memory of mantle lithosphere fabric — European LAB constrained from seismic anisotropy. *Lithos* 120, 131–143.
- Plomerová, J., Achauer, U., Babuška, V., Vecsey, L., 2007. Upper mantle beneath the Eger Rift (central Europe): plume or asthenosphere upwelling? *Geophys. J. Int.* 169, 675–682.
- Ratschbacher, L., Merle, O., Davy, P., Cobbold, P., 1991. Lateral extrusion in the eastern Alps, part 1: boundary conditions and experiments scaled for gravity. *Tectonics* 10, 245–256. <https://doi.org/10.1029/90TC02622>.
- Rosenberg, C.L., Brun, J.-P., Cagnard, F., Gapais, D., 2007. Oblique indentation in the Eastern Alps: insights from laboratory experiments. *Tectonics* 26 (TC2003). <https://doi.org/10.1029/2006TC001960>.

- Royden, L., Burchfiel, B.C., 1989. Are systematic variations in thrust belt style related to plate boundary processes? (The western Alps versus the Carpathians). *Tectonics* 8, 51–61. <https://doi.org/10.1029/TC008i001p00051>.
- Royden, L.H., Horváth, F., Burchfiel, B.C., 1982. Transform faulting, extension, and subduction in the Carpathian Pannonian region. *Bull. Geol. Soc. Am.* 93, 717–725.
- Sambridge, M., 1999. Geophysical inversion with a neighbourhood algorithm – I. Searching a parameter space. *Geophys. J. Int.* 138, 479–494.
- Scharf, A., Handy, M.R., Favaro, S., Schmid, S.M., Bertrand, A., 2013. Modes of orogen-parallel stretching and extensional exhumation in response to microplate indentation and roll-back subduction (Tauern Window, Eastern Alps). *Int. J. Earth Sci.* 102, 1627–1654. <https://doi.org/10.1007/s00531-013-0894-4>.
- Schmid, S.M., Aebli, H.R., Heller, F., Zingg, A., 1989. The role of the periadriatic Line in the tectonic evolution of the Alps. In: Coward, M.P., Dietrich, D., Park, R.G. (Eds.), *Alpine Tectonics*. Geol. Soc. London Spec. Publ. 45pp. 153–171.
- Schmid, S.M., Pfiffner, O.A., Froitzheim, N., Schönborn, G., Kissling, E., 1996. Geophysical-geological transect and tectonic evolution of the Swiss-Italian Alps. *Tectonics* 15, 1036–1064. <https://doi.org/10.1029/96TC00433>.
- Schmid, S.M., Fügenschuh, B., Kissling, B., Schuster, R., 2004. Tectonic map and overall architecture of the Alpine orogen. *Ecolgea geol. Helv.* 97, 93–117. <https://doi.org/10.1007/s00015-004-1113-x>.
- Schmid, S.M., Scharf, A., Handy, M.R., Rosenberg, C.L., 2013. The Tauern Window (Eastern Alps, Austria): a new tectonic map, with cross-sections and a tectonometamorphic synthesis. *Swiss J. Geosci.* 106, 1–32. <https://doi.org/10.1007/s00015-013-0123-y>.
- Schuster, R., Koller, F., Hoek, V., Hoinkes, G., Bousquet, R., 2004. Explanatory notes to age map of the metamorphic structure of the Alps—metamorphic evolution of the Eastern Alps. *Mitteilungen der Österreichischen Mineralogischen Gesellschaft* 149, 175–199.
- Shiomi, K., Park, J., 2008. Structural features of the subducting slab beneath the Kii Peninsula, central Japan: seismic evidence of slab segmentation, dehydration, and anisotropy. *J. Geophys. Res.* 113 (B10318). <https://doi.org/10.1029/2007JB005535>.
- Siebel, W., Blaha, U., Chen, F., Rohrmüller, J., 2005. Geochronology and geochemistry of a dyke-host rock association and implications for the formation of the Bavarian Pfahl shear zone, Bohemian Massif. *Int. J. Earth. Sci. (Geol. Rundsch.)* 94, 8–23.
- Siebel, W., et al., 2010. Age constraints on faulting and fault reactivation: a multi-chronological approach. *Int. J. Earth Sci.* 99, 1187–1197.
- Singer, J., Kissling, E., Diehl, T., Hetényi, G., 2017. The underthrusting Indian crust and its role in collision dynamics of the Eastern Himalaya in Bhutan: insights from receiver function imaging. *J. Geophys. Res.* 122, 1152–1178. <https://doi.org/10.1002/2016JB013337>.
- Spada, M., Bianchi, I., Kissling, E., Piana Agostinetti, N., Wiemer, S., 2013. Combining controlled-source seismology and receiver function information to derive 3-D Moho topography for Italy. *Geophys. J. Int.* 194, 1050–1068. <https://doi.org/10.1093/gji/ggt148>.
- Stucchi, M., et al., 2012. The SHARE European Earthquake Catalogue (SHEEC) 1000–1899. *J. Seismol.* 17, 523–544. <https://doi.org/10.1007/s10950-012-9335-2>.
- TRANSALP Working Group, 2002. First deep seismic reflection images of the Eastern Alps reveal giant crustal wedges and transcrustal ramps. *Geophys. Res. Lett.* 29, 92.1–92.4. <https://doi.org/10.1029/2002GL014911>.
- Vecsey, L., Plomerová, J., Jedlička, P., Munzarová, H., Babuška, V., AlpArray Working Group, 2017. Data quality control and tools in passive seismic experiments exemplified on Czech broad-band seismic pool MOBNET in the AlpArray collaborative project. *Geosci. Instrum. Method. Data Syst.* 6, 505–521. <https://doi.org/10.5194/gi-6-505-2017>.
- Weber, J., Vrabec, M., Pavlovčič-Prešeren, P., Dixon, T., Jiang, Y., Stopar, B., 2010. GPS-derived motion of the Adriatic microplate from Istria Peninsula and Po Plain sites, and geodynamic implications. *Tectonophysics*. 483, 214–222.
- Žák, J., Verner, K., Janoušek, V., Holub, F.V., Kachlík, V., Finger, F., Hajná, J., Tomek, F., Vondrovic, L., Trubač, J., 2014. A plate-kinematic model for the assembly of the Bohemian Massif constrained by structural relationships around granitoid plutons In: Schulmann, K. et al. (eds.), *The Variscan Orogeny: Extent, Timescale and Formation of the European Crust*. London Geol. Soc. Spec. Publ. 405, 169–196. doi:<https://doi.org/10.1144/SP405.9>.
- Zandt, G., Ammon, C., 1995. Continental crust composition constrained by measurements of crustal Poisson's ratio. *Nature* 374, 152–154.
- Zandt, G., Myers, S.C., Wallace, T.C., 1995. Crust and mantle structure across the Basin and Range-Colorado Plateau boundary at 37°N latitude and implications for Cenozoic extensional mechanism. *J. Geophys. Res.* 100, 10529–10548. <https://doi.org/10.1029/94JB03063>.
- Zhu, L.P., 2000. Crustal structure across the San Andreas Fault, southern California from teleseismic converted waves. *Earth Planet. Sci. Lett.* 179, 183–190. [https://doi.org/10.1016/S0012-821X\(00\)00101-1](https://doi.org/10.1016/S0012-821X(00)00101-1).
- Zhu, L., Kanamori, H., 2000. Moho depth variation in southern California from teleseismic receiver functions. *J. Geophys. Res.* 105, 2969–2980.